PHILOSOPHICAL TRANSACTIONS OF THE ROYAL SOCIETY A MATHEMATICAL, PHYSICAL & ENGINEERING SCIENCES

Dynamical X-ray Diffraction from Imperfect Crystals in the Bragg Case-Extinction and the Asymmetric Limits

S. W. Wilkins

Phil. Trans. R. Soc. Lond. A 1981 **299**, 275-317
doi: 10.1098/rsta.1981.0024

DYNAMICAL X-RAY DIFFRACTION FROM IMPERFECT CRYSTALS IN THE BRAGG CASE – EXTINCTION AND THE ASYMMETRIC LIMITS

By S. W. WILKINS

C.S.I.R.O. Division of Chemical Physics, P.O. Box 160, *Clayton, Victoria, Australia* 3168

(*Communicated by Sir Peter Hirsch, F.R.S. – Received* 28 *March* 1980)

CONTENTS

Vol. 299. A 1448. 20 [Published 11 February 1981

The variation of X-ray Bragg-reflexion properties of uniformly bent and mosaic-imperfect crystals is systematically explored within the framework of the Takagi–Taupin equations by using spherical-wave boundary conditions. For simplicity, consideration is restricted to centrosymmetric crystals with zero anomalous dispersion, although the methods used are quite general. For uniformly bent crystals, the diffraction properties are explored as functions of the bending radius, $\bar{R}$, and the asymmetry parameter, $\beta = \cot\theta_B \tan\alpha$, where θ_B is the Bragg angle and α is the asymmetry angle. For mosaic crystals, the diffraction properties are explored as functions of (i) the block size (assumed uniform), ℓ, (ii) the standard deviation of the mosaic-block tilt distribution, σ_b, (iii) the standard deviation of the mosaic shift distribution, σ_c, and (iv) the asymmetry parameter, β. From these results, strong evidence is obtained for the universal nature of the asymmetric limits as zero-extinction (kinematical) limits, and, moreover, that the limits are attained in such a manner that the imperfect-crystal result (for intensity along the surface and therefore also for the integrated reflectivity) first tends asymptotically to the corresponding dynamical-theory result for a perfect crystal, before finally tending to the kinematical value in the limit.

The relevance of the present work to the conventional approach to the extinction problem is discussed, and various limiting cases of the general mosaic-block model (g.m.b.m.) are explored. In particular, pure primary and secondary extinction are considered. On the problem of understanding the diffraction behaviour in the asymmetric limits, an examination of the results suggests that the conventional classification scheme for types of extinction is incomplete and that a third type of secondary extinction, at least, should be added to the classification scheme. This third type arises owing to angular spreading-out of the diffracted beam as it passes through the crystal, and the possibility of its occurrence is excluded in the formulation of the Darwin transfer equations.

1. Introduction

The complicating effect of dynamical scattering (or extinction) on the determination of structure-factor values from X-ray diffraction reflectivities has been appreciated since the earliest days of such measurements. In two classic papers, Darwin (1914 *a*, *b*) proposed two theories to describe X-ray diffraction reflectivities. The first (Darwin 1914*a*), later referred to as the kinematical theory, involved single scattering from the primary beam which was attenuated only by absorption as it passed through the crystal. This theory had the physically unobtainable result that, for a sufficiently thick crystal, the reflectivity could exceed unity. Darwin then proposed a second theory, subsequently designated the dynamical theory, which treated the amplitude coupling between the transmitted and diffracted beams as they passed through an assumed perfect crystal.

Neither theory, however, was capable of describing adequately the integrated reflectivity data for rock-salt obtained by Bragg *et al.* (1921 *a*, *b*), especially for the strongest reflexions. Darwin (1922) appreciated that the problem lay 'in the imperfections of the crystals and [that] this introduces many complications'. In this third classic paper, Darwin gave a general treatment of X-ray diffraction from imperfect crystals which has provided the framework for nearly all subsequent theoretical approaches (see, for example, Werner & Arrott 1965; Werner *et al.* 1966; Zachariasen 1967; Becker & Coppens 1974) to the extinction problem in crystallography. In this work, Darwin (i) introduced the mosaic-block model of crystal structure, (ii) elaborated the concept of extinction, which he subdivided into primary and secondary contributions, and (iii) developed the intensity-coupling equations for calculating the effect of secondary extinction. Darwin also presented solutions to the transfer equations for some cases and, in particular, for the asymmetric Bragg case (his equation (7.2)).

Applications of the Darwin approach to small crystals have been made by Zachariasen (1967) and Becker & Coppens (1974), and their results are widely used in structure-factor refinements. However, the effects and the domain of validity of many of the assumptions made in these theories are difficult to assess. Moreover, their methods are essentially directed towards the aim of *correcting for* the effect of extinction by modelling the inner morphology of the crystal specimen. Recently, Mathieson (1976, 1977 *a*, *b*, 1979 *a*) has outlined a general approach to the extinction problem which is directed towards the *elimination* of extinction by experimental means. The approach is based on the identification of universal limits where the integrated reflectivity attains the kinematical value (i.e. an extinction-free limit) independent of the structural state of the crystal, so that by making a series of measurements under controlled variation of an appropriate physical parameter, followed by extrapolation of the data to that limit, one can, in principle, obtain *extinction-free estimates* for structure-factor values (Mathieson 1979*a*). In this approach, attention is focused on the *level of interaction* rather than on the structural state of the crystal.

While the existence of universal extinction-free limits has been confirmed theoretically for *perfect crystals* (see, for example, Wilkins 1978*a*), the identification of universal extinction-free limits for *imperfect crystals* is still in need of detailed study. The present work is specifically directed towards studying the nature of X-ray diffraction from imperfect crystals within the framework of the Takagi–Taupin equations (see § 3). Special attention is given to the behaviour of extinction as a function of various parameters and, in particular, results (see §§ 7 and 8) for the behaviour of the level of extinction as a function of the degree of asymmetry (see figure 1) are presented for a range of imperfect crystal states. Mathieson's (1976, 1977*b*) postulate that the *asymmetric limit*

is in fact a universal extinction-free limit, which was originally demonstrated for perfect crystals (Hirsch & Ramachandran 1950; Mathieson 1977*b*; Wilkins 1978*a*, hereafter referred to as WI) is confirmed numerically for a large class of imperfect-crystal states (see §§ 7 and 8; a preliminary account of some of these findings was given by Wilkins (1980), hereafter referred to as WII).

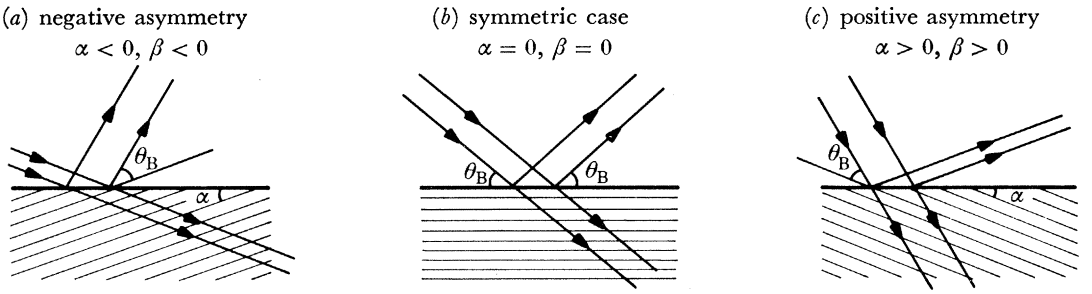

FIGURE 1. Bragg-reflexion scattering geometry for a semi-infinite crystal with an incident plane wave.

The present work, which invokes coherent dynamical diffraction from imperfect crystals, provides valuable insight into the functional dependence of extinction on the particular path through the crystal (see § 8) and also provides data which may be used to check the accuracy and range of applicability of available extinction theories (e.g., Zachariasen 1967; Becker & Coppens 1974; Kato 1976*a*, *b*, 1979, 1980).

2. NOTATION

For convenience, a glossary of the principal symbols used in the present work is given below:

General

(i) A single-bar superscript, for example as in $\bar{\ell}$, denotes that the quantity is measured in units of $|\kappa_{\mathrm{H}}|^{-1}$.

(ii) A double-bar superscript, for example as in $\bar{\bar{u}}_{\parallel}$, denotes that the quantity is measured in units of $|\boldsymbol{H}|^{-1}$.

Basic physical parameters

λ	wavelength of X-rays in vacuum
e	electronic charge
m	electronic mass
c	velocity of light
v	volume of unit cell (cm^3)
K	polarization factor; $K = 1$ for the component normal to the plane of diffraction and $K = \|\cos 2\theta\|$ for the parallel component.

Angles and indices

θ_{B}	Bragg angle (always assumed positive)
α	acute angle between crystal surface and reflecting planes (positive if the reflected beam is concentrated, see figure 1)
$\boldsymbol{H}$	stands for *hkl* reflexion, where *hkl* are Miller indices

Asymmetry parameter

β $= \cot\theta_B \tan\alpha \quad (-1 \leqslant \beta \leqslant 1)$

Coordinates

(s_O, s_H) oblique coordinates measured from entry point of spherical wave on surface and taken along directions of propagation of O and H beams, respectively (see figure 2)

(x_2, y_2) Cartesian coordinates taken in the plane of diffraction parallel and perpendicular to the Bragg planes, respectively (see figure 2)

(x_O, x_H) oblique coordinates perpendicular to the O and H beams, respectively

y_H coordinate perpendicular to the plane of diffraction

ξ distance along surface (see figure 2)

Structure factor and related parameters

F_H structure factor of index H

ψ_H $= -e^2 F_H \lambda^2/\pi mc^2 v$, Fourier component of index H of 4π times the polarizability

κ_H $= \lambda K e^2 F_H/mc^2 v = -\pi\psi_H/\lambda$

μ_0 $= 2\kappa''_O = -2\pi\psi''_O/\lambda$, linear absorption coefficient

$\bar{\mu}_0$ $= \mu_0/|\kappa_H| = -2g_0/(1+\ell^2)^{\frac{1}{2}}$, reduced linear absorption coefficient

g_0^{-1} $= -2|\kappa_H|/\mu_0(1+\ell^2)^{\frac{1}{2}}$, level of interaction in the symmetrical Bragg case (see WI)

p path length through the crystal as given by (4.11) and (4.12)

p_0 angular factor in path length as given by (4.11) and (4.12)

ℓ $= \kappa''_H/\kappa'_H$, anomalous dispersion parameter

Diffraction quantities

d_O, d_H field amplitudes inside crystal of forward-diffracted and diffracted beams, respectively

D_O, D_H field amplitudes outside crystal of beams travelling in forward diffracted and diffracted beam directions, respectively

D amplitude of the spherical wave as given by (4.2)

J_{h_1, p_1} displacement current at P_1 in direction h_1

ρ_H^s spherical wave integrated reflectivity as defined in (4.4)

ρ_H^p plane wave integrated reflectivity as defined in (4.5)

$\rho_H^{r.p.}$ random phase integrated reflectivity as given by (4.8)

$I(0)$ $= |D\kappa_H/\sin 2\theta_B|^2$, intensity at $\xi = 0$ (intensity in kinematical approximation with zero absorption)

y_{ext} $= 1 - \rho/\rho_{kin}$, extinction factor

Q integrated power diffracted per unit volume per unit intensity in the kinematical approximation as given by (4.14)

Q' effective value of Q in the presence of primary extinction

ξ_H extinction distance along the surface of the crystal and is given by (6.3)

A path length parameter in Zachariasen's treatment of the dynamical theory for a perfect crystal and is given by (9.2)

Structural quantities entering the Takagi–Taupin equations

$\boldsymbol{u}(s_O, s_H)$ displacement of medium at field point (s_O, s_H)
$u_\parallel$ component of medium displacement parallel to $\boldsymbol{H}$
G_H $= 2\pi \boldsymbol{H}\cdot\boldsymbol{u}(s_O, s_H)$, lattice phase factor

Structural parameters for imperfect crystal models

(i) *General*
f pairwise lattice phase correlation function as defined by (5.2)

(ii) *Uniformly-bent crystal*
$\bar{R}$ reduced radius of curvature

(iii) *General mosaic block model*
$\bar{\ell}$ side-length of the mosaic blocks in the plane of diffraction
σ_b standard deviation of the tilt distribution of the mosaic blocks
σ_c standard deviation of the shift distribution of the mosaic blocks

3. Theory of dynamical diffraction from imperfect crystals

The rigorous treatment of X-ray dynamical scattering from an imperfect crystal is a difficult problem. Kuriyama (1970, 1972) and Kuriyama & Miyakawa 1970) have made valuable contributions to this field via a quantum field-theoretical formulation of the problem. However, the numerical solution of Kuriyama's equations would seem to involve a large amount of computer time compared to the more approximate Takagi–Taupin equations (Takagi 1962, 1969; Taupin 1964; Kuriyama 1972), since Kuriyama's equations involve an extra angular variable describing the spreading-out of the diffracted beams due to crystal imperfections. For certain classes of models of an imperfect crystal, and particularly, for crystals containing slowly varying inhomogeneous strains or for crystals consisting of perfect-crystal mosaic blocks (the main class of imperfect crystal studied in this paper), one can expect the solution of the Takagi–Taupin equations to be very close to the correct solution. For mosaic block models, one might understand this to be so (see also Kuriyama 1972), because the Takagi–Taupin equations are essentially correct for a perfect crystal, and so should correctly treat the scattering within perfect-crystal mosaic blocks, while the boundary conditions between blocks may be incorporated via, say, an appropriate numerical solution procedure for the equations, as in the present work.

Recently, Kato (1976*a*, *b*; 1979) has shown that the Takagi–Taupin equations can be used to provide a unified treatment of primary and secondary extinction. In particular, Kato showed that for different values of the correlation length between lattice distortions, τ, one may obtain the perfect-crystal result (for $\tau \to \infty$), the ideally imperfect crystal result (for $\tau \to 0$), and a set of intensity-coupling equations (for τ small).

The work of the foregoing authors suggests that the Takagi–Taupin equations should provide a sound basis for treating dynamical scattering from a wide class of imperfect crystals, and in particular for investigating the trend in X-ray diffraction properties from imperfect crystals in the approach towards the asymmetric limits.

The form of the Takagi–Taupin equations with which we shall work is

$$\partial d_O/\partial s_O = \mathrm{i}\kappa_{-H} \exp(\mathrm{i}G_H)\, d_H, \tag{3.1a}$$

$$\partial d_H/\partial s_H = \mathrm{i}\kappa_H \exp(-\mathrm{i}G_H)\, d_O, \tag{3.1b}$$

where d_O and d_H are the wavefields of the direct and Bragg-reflected waves respectively, and κ_H is related to the structure factor F_H and the polarizability per unit volume, by

$$\kappa_H = \frac{\lambda K}{v}\frac{e^2}{mc^2}F_H = -\frac{\pi}{\lambda}\psi_H \tag{3.2}$$

(λ is the wavelength, K the polarization factor, v the unit-cell volume, e, m and c the usual constants, and κ'_H and κ''_H are the components of κ_H arising from the real and imaginary parts, respectively, of $\psi(\boldsymbol{r})$ which is 4π times the real-space polarizability).

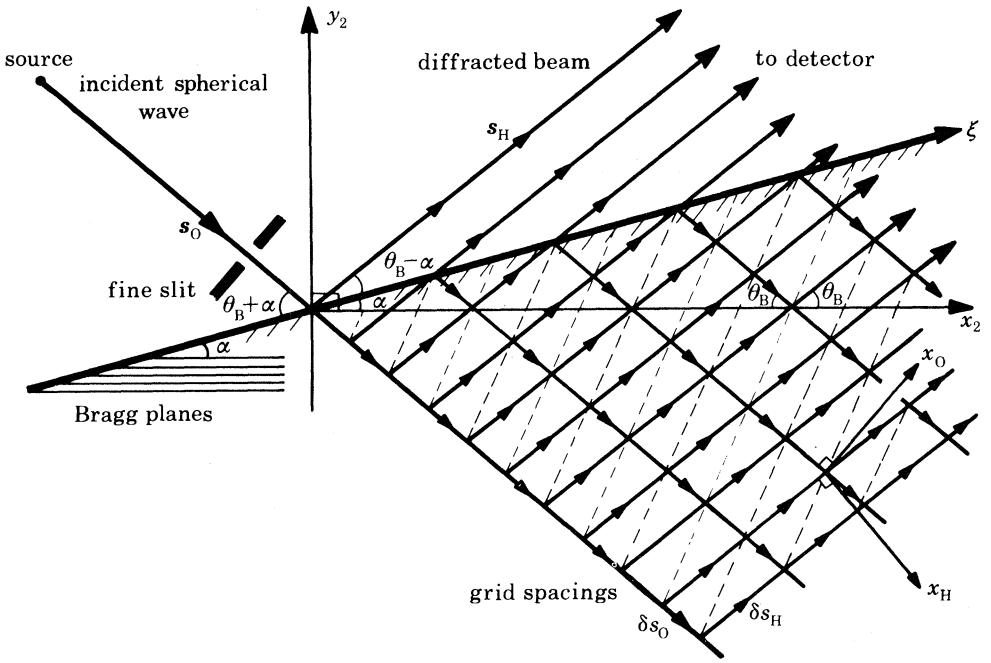

FIGURE 2. Scattering geometry in the plane of diffraction for the asymmetric Bragg case with an incident spherical wave. Also shown are multiple scattering paths in the crystal. The oblique dashed lines ('event lines') indicate loci of equal path length in the crystal; the numerical solution is propagated perpendicular to these lines. The vertices of the scattering paths occur as evaluation points in the numerical solution procedure.

The lattice phase factor G_H for the reflexion $\boldsymbol{H}$ is given by

$$G_H(s_O, s_H) = 2\pi \boldsymbol{H}\cdot\boldsymbol{u}(s_O, s_H), \tag{3.3}$$

where $\boldsymbol{u}(s_O, s_H)$ is the displacement of the medium at the field point (s_O, s_H). The choice of sign for the lattice phase factor in (3.1) and (3.3) is such as to conform with the definition of the structure factor as the Fourier transform (rather than the inverse transform) of the unit-cell electron-density distribution. It may be noted that a position in the plane of diffraction is specified by the oblique coordinates (s_O, s_H), the axes being taken along the directions of propagation of the O and H beams, respectively (see figure 2).

The equations (3.1) are the form of the Takagi–Taupin equations developed by Kato (1973), and will henceforth be called the T-equations. The details of the derivation of these equations together with the assumptions involved may be found in the papers of Takagi (1962, 1969), Taupin (1964), Kuriyama (1972) and Kato (1973). For our purposes, it is sufficient to point out that the following assumptions are involved in deriving (3.1): (i) the incident beam is

monochromatic, (ii) the two-beam approximation is valid, (iii) the quartic dispersion relation may be approximated adequately by the usual quadratic form, with a consequence that the possibility of specular reflexion is excluded, (iv) the two components of polarization may be treated separately.

(*a*) *Symmetry properties of the T-equations*

(i) *Uniform translation of the medium*

If the medium is displaced by a uniform translation $\boldsymbol{a}$, then from (3.3) this leads to phase factors $\exp(2\pi i \boldsymbol{H}\cdot\boldsymbol{a})$ and $\exp(-2\pi i \boldsymbol{H}\cdot\boldsymbol{a})$ on the right sides of equations (3.1*a*) and (3.1*b*), respectively. Furthermore, if these phase factors are associated with the coupling constants κ in the respective equations, then one may equally well describe the displacement of the medium as a shift in the origin of the unit cell by $-\boldsymbol{a}$, involving the following transformation of the unit-cell coupling constant:

$$\kappa_{\mathrm{H}} \to \kappa_{\mathrm{H}} \exp(-2\pi i \boldsymbol{H}\cdot\boldsymbol{a}).$$

Such a change in origin of the unit cell will have no effect on measured intensities, although the phase of the diffracted beam may be affected (this can readily be seen, for example, from equations (14) of Kato (1976*a*)).

(ii) *Complex conjugation and wavevector reversal*

In quantum mechanics, the time-reversal operation and complex conjugation are very closely related (see, for example, Messiah 1965, p. 671). Similarly, the effect of complex conjugation on the T-equations is closely related to the reversal of the wavevectors of the forward and diffracted beams.

More specifically, if $d_{\mathrm{O}}(s_{\mathrm{O}}, s_{\mathrm{H}})$ together with $d_{\mathrm{H}}(s_{\mathrm{O}}, s_{\mathrm{H}})$ is a solution to (3.1), then

$$d^{\mathrm{r}}_{\mathrm{O}}(s^{\mathrm{r}}_{\mathrm{O}}, s^{\mathrm{r}}_{\mathrm{H}}) = d^{*}_{\mathrm{H}}(-s_{\mathrm{H}}, -s_{\mathrm{O}}); \quad d^{\mathrm{r}}_{\mathrm{H}}(s^{\mathrm{r}}_{\mathrm{O}}, s^{\mathrm{r}}_{\mathrm{H}}) = d^{*}_{\mathrm{O}}(-s_{\mathrm{H}}, -s_{\mathrm{O}}) \tag{3.4}$$

is also a solution to (3.1) (cf. equation XV.72 in Messiah (1965)), where the superscript r denotes the wavevector-reversed solution and coordinates, and an asterisk denotes complex conjugation. Simply, this solution corresponds to running the scattering problem backwards (see figure 3).

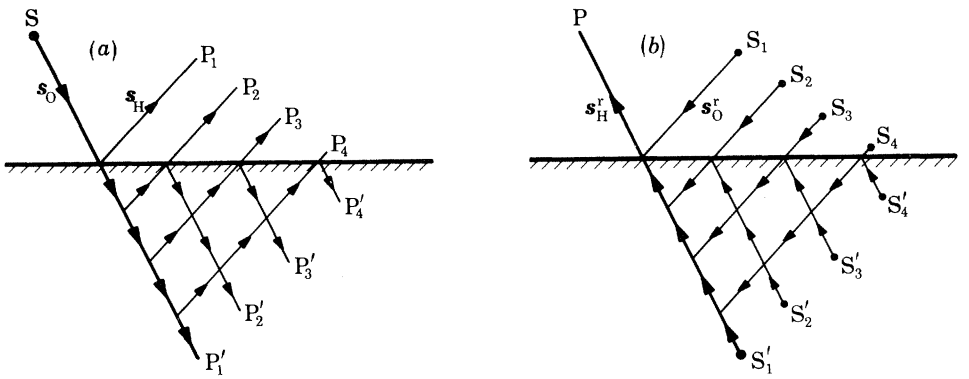

FIGURE 3. Scattering arrangements for a solution, (*a*), and the corresponding wavevector-reversed solution, (*b*), with sources denoted by the letter S and observation points denoted by the letter P.

(iii) *Reciprocity and microscopic reversibility*

Closely related to the idea of wavevector reversal is the so-called reciprocity theorem. This theorem was introduced in optics by Lorentz (1905) and later introduced into the X-ray diffrac-

tion context by von Laue (1935). Essentially the theorem states (see, for example, Kato 1968) that, when a radiation source having a direction $\boldsymbol{h}_1$ of polarization and located at P_1 excites a current $\boldsymbol{J}^{(1)}_{\boldsymbol{h}_2, P_2}$ at P_2 in a direction $\boldsymbol{h}_2$, then a radiation source of the same strength and of direction $\boldsymbol{h}_2$ of polarization, located at P_2, excites a current $\boldsymbol{J}^{(2)}_{\boldsymbol{h}_1, P_1}$ at P_1, in the direction $\boldsymbol{h}_1$, i.e.

$$\boldsymbol{J}^{(1)}_{\boldsymbol{h}_2, P_2} = \boldsymbol{J}^{(2)}_{\boldsymbol{h}_1, P_1}; \tag{3.5}$$

no other component of current is excited at P_1, except in the direction $\boldsymbol{h}_1$. Moreover, when P_1 and P_2 are both outside the crystal (as in this work), the result holds in the presence of absorption; if, as in von Laue's treatment, the currents at points P_1 and P_2 arise only from the displacement current $(1/4\pi)\,\partial \boldsymbol{D}/\partial t$, then, for a monochromatic wave, (3.5) is equivalent to the equation

$$\boldsymbol{D}^{(1)}_{\boldsymbol{h}_2, P_2} = \boldsymbol{D}^{(2)}_{\boldsymbol{h}_1, P_1}. \tag{3.6}$$

It should be noticed from (3.6) that the field amplitudes, for the two configurations discussed, are *equal in amplitude and phase*. An illustration of the reciprocity theorem is given in figure 4.

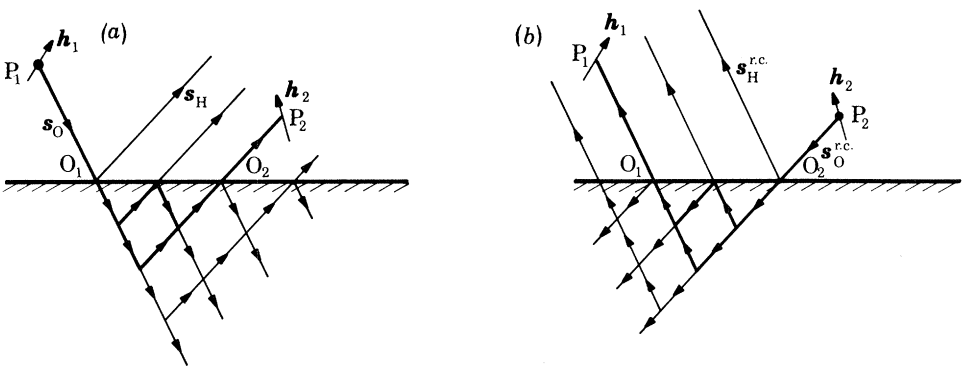

FIGURE 4. Scattering arrangements for (*a*) a solution with a spherical wave emanating from P_1 and the diffracted amplitude detected at P_2, and (*b*) a solution involving the reciprocal arrangement with the source at P_2 and the diffracted amplitude detected at P_1. The thicker-line scattering paths indicate possible scattering paths between P_1 and P_2, and are the same in (*a*) and (*b*).

A stronger version of the reciprocity theorem has been established by Moodie (1972) for many beam electron diffraction through a perfect-crystal plate. Moodie extended the reciprocity result to individual scattering processes (diagrams) and was able to show that, to every individual scattering process in an arbitrary orientation, there exists a process in the reciprocity configuration equal in amplitude and phase.

It is not difficult to see that a similar result also obtains within the framework of the T-equations for X-ray diffraction from imperfect crystals. Briefly, after Kato (1976*a*), one may write, for the amplitude of the diffracted beam at the exit point (s^e_O, s^e_H), the expression

$$d_H(s^e_O, s^e_H) = \sum_R B^H_R \exp(iQ_R), \tag{3.7}$$

where the amplitude for the scattering path R is

$$B^H_R = (D/\delta s_H \sin 2\theta_B)\,(i\kappa_H \delta s_H)\,(-\kappa_H \delta s_H \kappa_{-H} \delta s_O)^r, \tag{3.8}$$

and the phase for the scattering path R is

$$Q_R = -G(s^1_O, 0) + G(s^2_O, s^2_H) - \ldots + G(s^r_O, s^r_H) - G(s^{r+1}_O, s^r_H) \quad (s^{r+1}_O = s^e_O), \tag{3.9}$$

with δs_O and δs_H being the grid-spacing vectors along the transmitted and diffracted beam directions, respectively, D being the amplitude of the incident spherical wave (see equation (25), Kato (1976*a*) and also equation (4.2*a*) in the present work), and r denoting the number of scatterings in the path R from the diffracted-beam into the transmitted-beam direction. If one defines the reciprocity configuration (see figure 4) by interchanging the point of entry of the incident beam and the point of emergence of the diffracted beam, one then has that the direction of the diffracted beam in the original configuration is opposite in sense to that of the incident beam exciting diffraction in the reciprocity configuration, so that one has the transformation

$$\left.\begin{aligned}\delta \boldsymbol{s}_O &\to -\delta \boldsymbol{s}_H = \delta \boldsymbol{s}_O^{\text{r.c.}},\\ \delta \boldsymbol{s}_H &\to -\delta \boldsymbol{s}_O = \delta \boldsymbol{s}_H^{\text{r.c.}},\end{aligned}\right\} \tag{3.10}$$

with the superscript r.c. denoting quantities in the reciprocity configuration. It immediately follows from (3.8) and (3.10) that

$$B_R^H = (B_R^H)^{\text{r.c.}}, \tag{3.11}$$

provided the amplitudes of the incident spherical waves are equal in the two cases. Moreover, it follows from (3.9) that the phases will be equal provided the phases of the incident beams are equal, since the same vertices occur in (3.9) in each case (see figure 4), and the order in which they are encountered (i.e. forward or backward) does not affect Q_R. Note, for a finite thickness crystal, this result does *not* imply that the forward-diffracted amplitude emerging from the lower surface of the crystal is equal in each case.

The principle of reciprocity outlined above is analogous to the principle of microscopic reversibility in quantum mechanics (see, for example, Messiah 1965, p. 673). The reciprocity principle has proved very useful in helping to understand various diffraction problems. For example, in electron diffraction it has been used to devise tests for symmetry operators via convergent-beam studies (Pogany & Turner 1968; Goodman 1975). In X-ray diffraction it has been used, for example, to relate intensity distributions in traverse-type topographs and section-type topographs (Kato 1968; Petrashen & Chukhovskii 1978). Application of the reciprocity principle will be made in § 4 of the present work to show the equality of mean integrated reflectivities for the positive and negative asymmetry cases.

(*b*) *Parametrization of the T-equations for a centrosymmetric crystal*

The form (3.1) of the T-equations is especially suited to spherical-wave boundary conditions (see, for example, Kato 1975), which in turn provide a very convenient method for calculating integrated reflectivities (see § 4 (*c*)). To simplify the notation in what follows, we shall rewrite equations (3.1) as

$$\frac{\partial d_O}{\partial \bar{s}_O} = \mathrm{i}\frac{\kappa_{-H}}{|\kappa_H|}\exp(\mathrm{i}G_H)\, d_H, \tag{3.12a}$$

$$\frac{\partial d_H}{\partial \bar{s}_H} = \mathrm{i}\frac{\kappa_H}{|\kappa_H|}\exp(-\mathrm{i}G_H)\, d_O, \tag{3.12b}$$

where $(\bar{s}_O, \bar{s}_H)$ denotes that the coordinates (s_O, s_H) are now measured in reduced units, $|\kappa_H|^{-1}$. Since the components of κ_H arising from real and imaginary parts of $\psi(\boldsymbol{r})$ are denoted by κ'_H and κ''_H respectively, then the reality of $\psi(\boldsymbol{r})$ implies that

$$\kappa'_{-H} = (\kappa'_H)^* \quad \text{and} \quad \kappa''_{-H} = (\kappa''_H)^*. \tag{3.13}$$

(i) *Anomalous dispersion*

Moreover, if the anomalous dispersion parameter is taken to be

$$\ell = \kappa''_{\mathrm{H}}/\kappa'_{\mathrm{H}} \quad (|\ell| \leqslant |g_0|), \tag{3.14}$$

and if consideration is restricted to structures possessing a centre of symmetry (and the origin of the unit cell is taken at such a centre of symmetry) then one has

$$\kappa_{\mathrm{H}} = \kappa_{-\mathrm{H}} = \kappa'_{\mathrm{H}} + \mathrm{i}\kappa''_{\mathrm{H}} = \kappa'_{-\mathrm{H}} + \mathrm{i}\kappa''_{-\mathrm{H}}, \tag{3.15}$$

with κ'_{H} and κ''_{H} both real and g_0 defined by (3.17). Thus, under these conditions, the coefficients in the T-equations (3.12) are dependent on the unimodular quantities

$$\frac{\kappa_{\mathrm{H}}}{|\kappa_{\mathrm{H}}|} = \frac{\kappa_{-\mathrm{H}}}{|\kappa_{\mathrm{H}}|} = \frac{1+\mathrm{i}\ell}{\mathrm{sgn}\,(\kappa'_{\mathrm{H}})\,(1+\ell^2)^{\frac{1}{2}}} = \frac{1+\mathrm{i}\ell}{(1+\ell^2)^{\frac{1}{2}}}, \tag{3.16}$$

where the sign function in (3.16) may be ignored (i.e. taken equal to 1), since, if κ'_{H} is negative, its effect in (3.1) or (3.12) may be equated to that of a uniform displacement of the medium, because $\mathrm{e}^{\mathrm{i}\pi} = \mathrm{e}^{-\mathrm{i}\pi} = -1$ (see § 3 (*a* i)).

(ii) *Normal absorption*

The form of the T-equations given in (3.1) and (3.12) is for unit refractive index and zero absorption, although absorption may very simply be included in the formulation of the equations. This is not done here because it turns out to be more convenient in computations to introduce later the absorption, in the equivalent manner that would be suggested by phenomenological considerations (see § 4 (*c*)). In our notation, the reduced linear absorption coefficient is given by

$$\bar{\mu}_0 = \mu_0/|\kappa_{\mathrm{H}}| = -2g_0/(1+\ell^2)^{\frac{1}{2}}, \tag{3.17}$$

where μ_0 is the usual linear absorption coefficient and g_0^{-1} is the level of interaction (in the symmetrical Bragg case) as defined by the second equality in (3.17) (see also WI).

4. Boundary conditions and geometrical parameters

For the present work the scattering geometry is that of the Bragg case (see figure 1) and the crystal will be taken to have a single mathematically flat surface (i.e. the crystal is semi-infinite in the direction normal to the surface).

To avoid certain divergence problems in the calculation of integrated reflectivities (consider, for example, the limit $\mu_0 \to 0$ in (4.13); see also WI), it will be assumed that the crystal has non-zero absorption. This is not a severe restriction, however, since all real crystals have some finite absorption.

(*a*) *Asymmetry*

An important geometrical parameter chosen for investigation in this study is the degree of asymmetry. The asymmetry angle α is defined as the acute angle between the surface and the mean orientation of the Bragg planes under consideration, such that for grazing incidence $\alpha < 0$ while for grazing emergence $\alpha > 0$ (see figure 1). The symmetrical case occurs when $\alpha = 0$. As in our previous papers, the degree of asymmetry will be specified by the parameter

$$\beta = \cot\theta_{\mathrm{B}} \tan\alpha, \quad -1 \leqslant \beta \leqslant 1. \tag{4.1}$$

Note that the natural limits of α are $\pm\theta_B$, corresponding to $\beta = \pm 1$, and that, for a given suitably cut crystal, the parameter β can be varied continuously throughout this range by rotating the crystal about the normal to the reflecting planes (see, for example, Mathieson 1975).

(*b*) *Spherical-wave boundary conditions*

For calculations the boundary conditions at the crystal surface will be taken to be those applying to a spherical incident wave, in the form discussed, for example, by Kato (1961) and Saka *et al.* (1972), namely

$$D_O(s_O, s_H) = (D/\sin 2\theta_B)\,\delta(s_H) = D\delta(x_O), \tag{4.2a}$$

$$D_H(s_O, 0) = 0, \tag{4.2b}$$

where capital letters are used to denote wavefields outside the crystal, D is the amplitude of the spherical wave and (x_O, x_H) are the coordinates perpendicular to the O and H beams respectively (see figure 2), and are equal to $\sin(2\theta_B)\,(s_H, s_O)$. Note that expressions (4.2) are in fact mathematical devices for calculating diffraction properties and should not be used to deduce incident-beam properties (see, for example, Kato 1975). In practice, the spherical wave boundary conditions are closely approximated for a conventional X-ray source when a fine slit (*ca.* 10 μm) is placed at a sufficiently large distance (*ca.* 1 m) from a very fine source, such that only one line of the characteristic spectrum is able to satisfy the Bragg condition, yet the angular variation of intensity in the incident beam is uniform over the full angular range of the rocking curve. The resulting intensity distribution along the surface of the crystal (see figure 2) is called a *section topograph* (see, for example, Authier 1977).

(*c*) *Integrated reflectivity*

For a spherical wave source (4.2) at (x'_O, x'_H), let $d^s_H(x''_O, x''_H; x'_O, x'_H)$ be the solution at (x''_O, x''_H) on the exit surface of the crystal. Then the corresponding plane-wave solution for unit incident amplitude ($D = 1$) in the plane of diffraction is (Kato 1976*a*)

$$d^p_H(x''_O, x''_H; K_x) = \int \mathrm{d}x'_O \exp(\mathrm{i}K_x x'_O)\, d^s_H(x''_O, x''_H; x'_O, x'_H), \tag{4.3}$$

where K_x is the component of the wavevector $\boldsymbol{K}$ ($|\boldsymbol{K}| = 2\pi/\lambda$) in the plane of diffraction and lying parallel to the x_O-axis. Thus, the unit-incident-amplitude plane-wave solution is exactly the Fourier transform of the corresponding unit-amplitude (see (4.2*a*)) spherical-wave solution. *Note, however, that we cannot assume* d^s_H *to be translationally invariant, since we intend to treat imperfect crystals.*

The vacuum wave field amplitude, say $D_H(X_O, X_H; x'_O, x'_H)$, at an observation point (X_O, X_H) outside the crystal (all denoted by symbols with capital letters) differs only by a phase factor from the crystal amplitude $d_H(x''_O, x''_H; x'_O, x'_H)$ at the corresponding exit point (x''_O, x''_H) on the surface of the crystal. Thus, based on Kato (1974, p. 323; 1976*a*), one may write for the spherical-wave integrated reflectivity in the Bragg case considered here

$$\rho^s_H(\xi') = \lambda \sin(\theta_B - \alpha) \iint \mathrm{d}\xi''\, \mathrm{d}y_H\, |d^s_H(\xi''; \xi')|^2, \tag{4.4}$$

and for the plane-wave integrated reflectivity

$$\rho_{\mathrm{H}}^{\mathrm{p}} = \lambda \sin(\theta_{\mathrm{B}} - \alpha)\, L^{-1} \int_{-\frac{1}{2}L}^{\frac{1}{2}L} \mathrm{d}\xi' \iint \mathrm{d}\xi''\, \mathrm{d}y_{\mathrm{H}}\, |d_{\mathrm{H}}^{\mathrm{s}}(\xi''; \xi')|^2, \tag{4.5a}$$

$$\equiv \lambda \sin(\theta_{\mathrm{B}} - \alpha) \left\langle \iint \mathrm{d}\xi''\, \mathrm{d}y_{\mathrm{H}}\, |d_{\mathrm{H}}^{\mathrm{s}}(\xi''; \xi')|^2 \right\rangle_L, \tag{4.5b}$$

with $L \to \infty$, where L is the extent of the plane wave along the surface (i.e. the ξ-axis in figure 2) and y_{H} refers to the axis perpendicular to the plane of diffraction. The expectation value introduced in (4.5*b*) is the average over the entry points on the surface and is given, for a general function $F(\xi)$, by

$$\langle F \rangle_L = L^{-1} \int_{-\frac{1}{2}L}^{\frac{1}{2}L} \mathrm{d}\xi\, F(\xi). \tag{4.6}$$

From (4.4) and (4.5*b*), one has the relation

$$\rho_{\mathrm{H}}^{\mathrm{p}} = \langle \rho_{\mathrm{H}}^{\mathrm{s}}(\xi') \rangle_{L \to \infty}, \tag{4.7}$$

between plane-wave and spherical-wave integrated reflectivities.

If spherical waves of the form (4.2) had been homogeneously distributed with a unit intensity per unit length along the entry surface *without* any definite phase relation, one would also have obtained the integrated reflectivity (denoted for this case by the superscript r.p.) as

$$\rho_{\mathrm{H}}^{\mathrm{r.p.}} = \langle \rho_{\mathrm{H}}^{\mathrm{s}}(\xi') \rangle_{L \to \infty}. \tag{4.8}$$

This case is claimed by Kato (1976*a*) to be the most realistic for conventional diffractometry, in which the crystal is illuminated by a wide homogeneous beam.

If we now explicitly include the effect of normal absorption (since we have previously chosen to formulate the T-equations in the absence of normal absorption) and if we assume negligible spreading-out of the diffracted beam perpendicular to the plane of diffraction, we may write the following expressions for the integrated reflectivities:

$$\rho_{\mathrm{H}}^{\mathrm{s}}(\xi') = \lambda \sin(\theta_{\mathrm{B}} - \alpha) \int_{\xi'}^{\infty} \mathrm{d}\xi'' \exp(-\mu_0 p_0 |\xi'' - \xi'|)\, |d_{\mathrm{H}}^{\mathrm{s}}(\xi''; \xi')|^2 \tag{4.9}$$

and

$$\rho_{\mathrm{H}}^{\mathrm{p}} = \lambda \sin(\theta_{\mathrm{B}} - \alpha) \left\langle \int_{-\infty}^{\infty} \mathrm{d}\xi'' \exp(-\mu_0 p_0 |\xi'' - \xi'|)\, |d_{\mathrm{H}}^{\mathrm{s}}(\xi''; \xi')|^2 \right\rangle_{L \to \infty}, \tag{4.10}$$

where the coordinate ξ measures the distance along the surface of the crystal (see figure 2), and the unique scattering path length p connecting ξ' and ξ'' is given by

$$p(\xi'' - \xi'; \theta_{\mathrm{B}}, \alpha) = [\sin(2\theta_{\mathrm{B}})]^{-1} [\sin(\theta_{\mathrm{B}} - \alpha) + \sin(\theta_{\mathrm{B}} + \alpha)]\, |\xi'' - \xi'| \tag{4.11}$$

$$= p_0(\theta_{\mathrm{B}}, \alpha)\, |\xi'' - \xi'|. \tag{4.12}$$

As a simple illustration of the application of (4.10), we consider the kinematical approximation for which $|d_{\mathrm{H}}^{\mathrm{s}}(\xi''; \xi')|^2 = |D\kappa_{\mathrm{H}}/\sin 2\theta_{\mathrm{B}}|^2$, so that, for a sufficiently thick absorbing platelet treated in the Bragg case, we have the standard result (James 1949)

$$\rho_{\mathrm{H,\,kin}}^{\mathrm{p}} = \rho_{\mathrm{H,\,kin}}^{\mathrm{s}} = \rho_{\mathrm{H,\,kin}}^{\mathrm{r.p.}} = \frac{\lambda}{\sin 2\theta_{\mathrm{B}}} \frac{|\kappa_{\mathrm{H}}|^2}{\mu_0} \tfrac{1}{2}(1 - \beta) = \tfrac{1}{2}(1 - \beta) \frac{Q}{\mu_0}, \tag{4.13}$$

where Q is the usual integrated power diffracted per unit volume per unit intensity in the kinematical approximation, and is given by

$$Q = \frac{\lambda^3}{v^2} \frac{K^2 |F_{\mathrm{H}}|^2}{\sin 2\theta_{\mathrm{B}}} \left(\frac{e^2}{mc^2}\right)^2 = \frac{\lambda |\kappa_{\mathrm{H}}|^2}{\sin 2\theta_{\mathrm{B}}}. \tag{4.14}$$

(*d*) *Extinction factor*

A result, that conventionally provides a reference value for integrated reflectivity measurements on imperfect crystals, is that of the integrated reflectivity of an ideally imperfect (or perfectly mosaic) crystal (Bragg *et al.* 1926). While the concept of the ideally imperfect crystal is itself imperfect (see, for example, Hart 1974, and Mathieson 1978), it is made operationally meaningful by tying it to the integrated reflectivity, ρ_{kin}, that would obtain if the simple kinematical approximation were valid. It is the ratio of an actual ρ to ρ_{kin} which forms the basis for a convenient measure of extinction, namely the extinction factor

$$y_{\mathrm{ext}} = 1-\rho/\rho_{\mathrm{kin}}; \tag{4.15}$$

this coincides with the definition used in our previous work. For the present case of interest, namely the thick-crystal asymmetric Bragg case, the appropriate form of ρ_{kin} is (4.13) both for plane-waves and for spherical waves. The behaviour of y_{ext} forms a central area of investigation in the present work.

For the asymmetric Bragg case being considered, the extinction factors corresponding to (4.9) and (4.10) are explicitly given by

$$y^{\mathrm{s}}_{\mathrm{ext}}(\xi') = 1-\frac{\int_{\xi'}^{\infty} \mathrm{d}\xi'' \exp(-\mu_0 p)\,|d^{\mathrm{s}}_{\mathrm{H}}(\xi'';\xi')|^2}{|\kappa_{\mathrm{H}}|^2 \sin 2\theta_{\mathrm{B}}/\mu_0[\sin(\theta_{\mathrm{B}}+\alpha)+\sin(\theta_{\mathrm{B}}-\alpha)]} \tag{4.16}$$

and

$$y^{\mathrm{p}}_{\mathrm{ext}} = 1-\frac{\int_{-\infty}^{\infty} \mathrm{d}\xi'' \exp(-\mu_0 p)\,\langle|d^{\mathrm{s}}_{\mathrm{H}}(\xi'';\xi')|^2\rangle_{L\to\infty}}{|\kappa_{\mathrm{H}}|^2 \sin 2\theta_{\mathrm{B}}/\mu_0[\sin(\theta_{\mathrm{B}}+\alpha)+\sin(\theta_{\mathrm{B}}-\alpha)]} \tag{4.17}$$

respectively, so that

$$y^{\mathrm{p}}_{\mathrm{ext}} = \langle y^{\mathrm{s}}_{\mathrm{ext}}(\xi')\rangle_{L\to\infty}. \tag{4.18}$$

In deriving (4.16) and (4.17), we have used equations (4.9)–(4.13).

(*e*) *Symmetry with respect to reversal in sign of the asymmetry parameter*

For perfect crystals it was pointed out in WI that Mathieson's (Mathieson 1975, 1976, 1977*b*) conjecture, that $\rho^{\mathrm{p}}/(1-\beta)$ (or equivalently $y^{\mathrm{p}}_{\mathrm{ext}}$) is even in β, is confirmed by conventional dynamical theory for both the infinite and finite thickness cases. It may be noted from the calculation leading from (4.10) to (4.13) that the factor $1-\beta$ essentially arises as a result of the cross-sectional area which the crystal surface presents to the diffracted beam.

One would like to know whether this symmetry result also applies to imperfect crystals. From the results already established it is possible to provide an answer to this question, within the framework of the T-equations, as follows.

First, we note that, if the asymmetry angle is α in a given scattering configuration, it will be $-\alpha$ in the reciprocity configuration (see § 3 (*a* iii)). Thus, by the reciprocity theorem for a given path R in the crystal, for the same amplitude source in each case, we have that

$$I^{+}_{\mathrm{R}}(\xi'';\xi') = I^{\mathrm{r.c.}}_{\mathrm{R}}(\xi';\xi'') = I^{-}_{\mathrm{R}}(\xi';\xi''), \tag{4.19}$$

where I^{+} and I^{-} are intensities calculated in the $+\alpha$ and $-\alpha$ asymmetry cases. Note that (4.19) applies equally well in the presence or absence of absorption since the path length p is the same for both the given configuration and the reciprocity configuration. For perfect crystals one may

assume translational invariance of I_R^+ and I_R^-, and immediately go on from (4.19) to prove with (4.17) (or (4.16)) that y_{ext} is *even* in β.

However, for imperfect crystals one cannot assume translational invariance of I_R^+ and I_R^- with respect to ξ, so that only the weaker result

$$\langle I_R^+(\xi''-\xi')\rangle_{L\to\infty} = \langle I_R^{r.c.}(\xi'-\xi'')\rangle_{L\to\infty} = \langle I_R^-(\xi'-\xi'')\rangle_{L\to\infty} \tag{4.20}$$

applies, where the mean is taken with respect to positions of the source, which for a statistically homogeneous medium will be equivalent to taking an ensemble average over crystal states for a given value of the source position, ξ'.

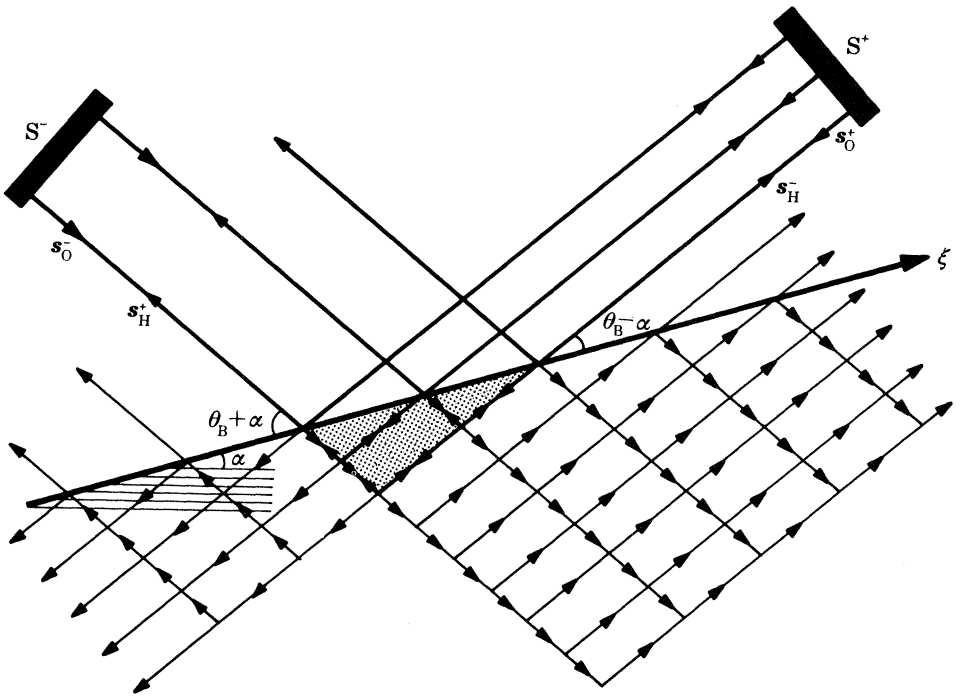

FIGURE 5. Positive, and corresponding negative, asymmetry cases for equal-width pseudo-plane-wave sources S^+ and S^-. The thicker-line scattering paths in the shaded region show the paths common to the two arrangements, while the thin lines show scattering paths that sample different regions of the crystal in each case.

Therefore, from (4.16) and (4.20), we immediately have the result that the *ensemble average of* y_{ext}^s *is invariant under reversal in sign of* β. From (4.17) and (4.20), we have, in principle, that y_{ext}^p is invariant under reversal in sign of β, provided L is sufficiently large, but in practice the necessarily finite extent of the incident wave means that the invariance will also only apply to the ensemble average of y_{ext}^p. Note that the invariance of the ensemble average of y_{ext} also applies if (4.8) is used for ρ.

Simply then, we see that, although equality obtains between intensities for a given path in the $+\alpha$ and $-\alpha$ configurations, different regions of the crystal contribute to ρ in the $+\alpha$ and $-\alpha$ cases (see figure 5), so that y_{ext} or $\rho/(1-\beta)$ are invariant, under reversal in sign of β, for an imperfect crystal only in the mean (the mean being either obtained via an ensemble average over crystal states or over entry points on the surface).

5. Structural models for imperfect crystals

It is only in a few idealized cases that detailed quantitative descriptions can be given of the precise structural state of a macroscopic real crystal. Such cases occur, for example, in synthetically grown Si single crystals having very low dislocation densities. In these crystals, the detailed defect configuration and lattice distortions may be analysed by X-ray topography (see, for example, Tanner 1976). More usually, the crystals studied in X-ray diffraction experiments consist of a very dense network of dislocations and distortions, and a detailed description of the structural state is impossible. At best, one might hope to describe an actual structural state in statistical terms of the number, clustering, and orientation of various types of defects or in terms of various displacement–displacement correlation functions (see, for example, Kato 1976*a*, *b*).

In treating the elastic X-ray scattering from imperfect crystals via the T-equations, the only way in which the state of perfection of the crystal enters the calculations is via the lattice phase factor $\exp \mathrm{i}G$ (see (3.1) and (3.3)). It is therefore central to the present aim of studying diffraction from imperfect crystals to decide on some appropriate, yet tractable, models for $\exp \mathrm{i}G$ or, more specifically, for the component of the continuum field-point displacement $\boldsymbol{u}$ lying parallel to $\boldsymbol{H}$ (the only component of $\boldsymbol{u}$ that is relevant in these calculations). Since the topic of dynamical diffraction from highly imperfect crystals is relatively unexplored, it seems sensible to consider models for types of imperfect crystal that are simple enough to be easily described mathematically, and yet to contain what are felt to be some of the essential components of the structural state of real imperfect crystals. The first model considered is that of the uniformly bent perfect crystal, while the second model considered is one involving a mosaic-block structure. The details of the models are as follows.

(*a*) *The uniformly bent crystal*

One of the simplest deviations from the perfect crystal state is that of a uniformly bent perfect crystal (the so-called uniform strain gradient case). For this model of a deformed crystal, analytic solutions to the T-equations have been obtained by several authors; in particular solutions for the Laue case have been obtained by Katagawa & Kato (1974), Petrashen & Chukhovskii (1976), Chukhovskii & Petrashen (1977), and for the Bragg case by Chukhovskii *et al.* (1978). The uniformly bent crystal is of particular interest because its state can be varied in a precise and controlled manner. It is partly as a result of this property that bent crystals have found widespread use as X-ray and neutron optical components such as monochromators (see, for example, Kohra *et al.* 1978).

The uniformly bent crystal model may be defined in operational terms as follows. Imagine a perfect crystal to be uniformly bent so that the Bragg planes become cylindrical surfaces with the axes of the cylinders lying in a direction normal to the plane of diffraction. The surface of the crystal is then ground, polished and etched until it is flat and undamaged. The angle between the surface and the tangent to the Bragg surfaces at the point of entry of an incident spherical wave is defined as the local asymmetry angle α (see figure 6).

Mathematically, the component of the displacement field parallel to the scattering vector $\boldsymbol{H}$ in the uniformly bent crystal is given, to a sufficient approximation, by

$$\bar{u}_{\parallel} = \tfrac{1}{2}\bar{R}^{-1}\bar{x}_2^2, \tag{5.1}$$

where $\bar{R}$ is the reduced radius of curvature, $\bar{x}_2$ is the reduced distance along the original undistorted Bragg planes, and a double bar over a symbol denotes that it is measured in reduced units $|H|^{-1} = \lambda/\sin\theta_B$.

It should be noted that, for a 'dynamically transparent' crystal (i.e., $\mathscr{k} = 0$) the diffraction properties are independent of the sign of $\bar{R}$ (see Chukhovskii *et al.* 1978, p. 615).

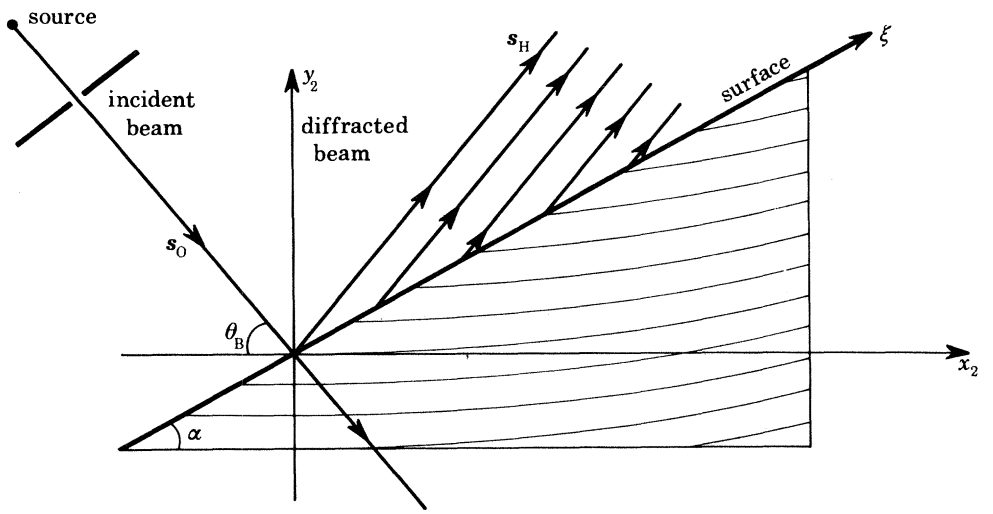

FIGURE 6. Scattering geometry and displacement field for the uniformly bent crystal models in the asymmetric Bragg case with spherical-wave boundary conditions.

(i) *Correlation function for the uniformly bent crystal*

We note that the uniformly bent crystal is an *inhomogeneous* model of an imperfect crystal, but with the simplifying property that the effect of translating the entry point along the surface of the crystal is equivalent to altering the asymmetry angle. This can be seen by examining the basic geometry (see figure 6). Useful parameters for describing the internal state of an imperfect crystal are the lattice phase correlation functions (Kato 1976*b*), the simplest of which is the pairwise correlation function, defined by

$$f(\Delta\bar{s}_O, \Delta\bar{s}_H; \bar{s}_O, \bar{s}_H) \equiv \langle \exp[iG(\bar{s}_O + \Delta\bar{s}_O, \bar{s}_H + \Delta\bar{s}_H)] \exp[-iG(\bar{s}_O, \bar{s}_H)] \rangle. \tag{5.2}$$

In the present model this correlation function is given trivially by

$$f(\Delta\bar{s}_O, \Delta\bar{s}_H; 0, 0) = \exp[-\tfrac{1}{2}i\bar{R}^{-1}(\Delta\bar{s}_O + \Delta\bar{s}_H)^2], \tag{5.3}$$

with fixed reference point taken at the entry point, (0, 0) of the spherical wave. Thus, we can see from (5.3) that the phase of f varies slowly for small $(\Delta\bar{s}_O, \Delta\bar{s}_H)$, but oscillates very rapidly for large values of $(\Delta\bar{s}_O, \Delta\bar{s}_H)$.

Practically, the uniformly bent crystal case may be achieved either mechanically (see, for example, Mathieson 1978) or by depositing an oxide layer on one side of a crystal plate (see, for example, Hashizume & Kohra 1971). Experimental results for the integrated reflectivity from uniformly bent crystals is contained in the work of Boeuf *et al.* (1978) and references cited therein. Some reasons for recent interest in studying bent crystals is in connection with the design of monochromators for synchrotron radiation (Boeuf *et al.* 1978; Kohra *et al.* 1978) and the dynamic focusing of X-rays (Petrashen & Chukhovskii 1976).

(*b*) *The general mosaic block model* (*g.m.b.m*)

In his seminal work on X-ray diffraction from imperfect crystals, Darwin (1922) assumed that the atoms of an imperfect crystal were 'arranged in blocks, each block a perfect crystal, but adjacent blocks not accurately fitted together'. This model was partly chosen for mathematical convenience as a discrete representation of a crystal involving inhomogeneous strains. Notwithstanding, mosaic block models have formed the basis for nearly all subsequent theoretical treatments of extinction in X-ray and neutron diffraction from imperfect crystals (Zachariasen 1967; Werner & Arrott 1965; Becker & Coppens 1974, see also Kato 1976*b*, model 2), an exception being the inhomogeneous-strain approach adopted by Kuriyama & Miyakawa (1970).

While the mosaic block model is obviously a highly idealized representation of the internal structural state of most crystals, there are cases where the mosaic block model appears to have direct physical manifestations (see, for example, Hirsch 1956; Barrett & Massalski 1966, p. 396, and references cited therein; Moodie & Warble 1980). Essentially, a mosaic block model concentrates all the dislocations in a small volume of a crystal into dislocations at the block or grain boundaries. Provided the blocks are not too large, this would seem a reasonable first approximation for use in the treatment of X-ray diffraction from real imperfect crystals.

In developing a mosaic block model for use in the present studies, we were guided by the following criteria.

(i) It was considered desirable that the model parameters be such as to allow the crystal state to be varied continuously from perfect to ideally imperfect states.

(ii) The model crystal should be statistically homogeneous, i.e. have mean structural properties independent of position in the crystal.

(iii) the crystal state should become ideally imperfect (i.e. $y_{\mathrm{ext}} \to 0$) as the block size goes to zero.

The general mosaic block model (g.m.b.m.) adopted in this work consists of the following components.

(i) *Block size* $\bar{\ell}$. The two-dimensional plane of diffraction is divided into square perfect-crystal blocks with side length $\bar{\ell}$.

(ii) *Block tilt* σ_{b}. The blocks are subject to an angular tilt about their centroids, which is sampled from a symmetrical triangular distribution with standard deviation σ_{b}.

(iii) *Block shift* σ_{c}. The blocks are subject to a displacement along the direction of the scattering vector $\boldsymbol{H}$ by an amount relative to their neighbours, which is sampled from a symmetrical triangular distribution with standard deviation σ_{c}. The shifts at a given block are calculated as the sum of independent random walks along the x_2- and y_2-directions, starting from an arbitrary origin block.

A schematic representation of a given configuration of the crystal in the g.m.b.m. is presented in figure 7. It should be noted that the blocks entirely fill the volume inside the bounding surfaces of the crystal, with no inter-block voids.

Mathematically, the component of the displacement field $\boldsymbol{u}$ along the direction of the scattering vector, $\boldsymbol{H}$, is given in the g.m.b.m. by

$$\bar{\bar{u}}_{\parallel}(x_2, y_2) = \sum_{i=1}^{I} c_i^x + \sum_{j=1}^{J} c_j^y + (b_I^x + b_J^y)\,(\bar{x} - \bar{x}_{IJ}), \tag{5.4}$$

where I and J are the block-lattice indices along the x_2- and y_2-directions (parallel and perpendicular to Bragg planes, respectively; see also figure 7) of the block containing the field point $(\bar{x}_2, \bar{y}_2)$.

The coordinate x_2 denotes the distance from the origin along the direction of the Bragg planes, with $\bar{x}_{IJ}$ being the x_2-coordinate of the centroid of the block at block site (I, J). Note that, for brevity, the subscript 2 is deleted from coordinates appearing on the right side of (5.4). The indices i and j run over the block-lattice sites from the origin to (I, J). The block shifts c_i^x and c_j^y are generated from a uniform (square) distribution such that the resulting triangular distribution of $c_i^x + c_j^y$ has standard deviation σ_c. The sum of the $c_i^x + c_j^y$ produces a random walk, the distribution of the sum tending to normal as the number of steps becomes large. The tilts b_I^x and b_J^y are also sampled from uniform distributions, and the resulting triangular distribution of $b_I^x + b_J^y$ has standard deviation σ_b. The units chosen for the parameters σ_b and σ_c are such that $\bar{\bar{u}}_{\|}$ is measured in units of $|\boldsymbol{H}|^{-1} = \lambda/\sin\theta_B$. The reason for choosing triangular distributions for the tilt and shift distributions is simply one of convenience in the numerical treatment, and is not considered to lead to specificity in any of the essential features of the results to be presented.

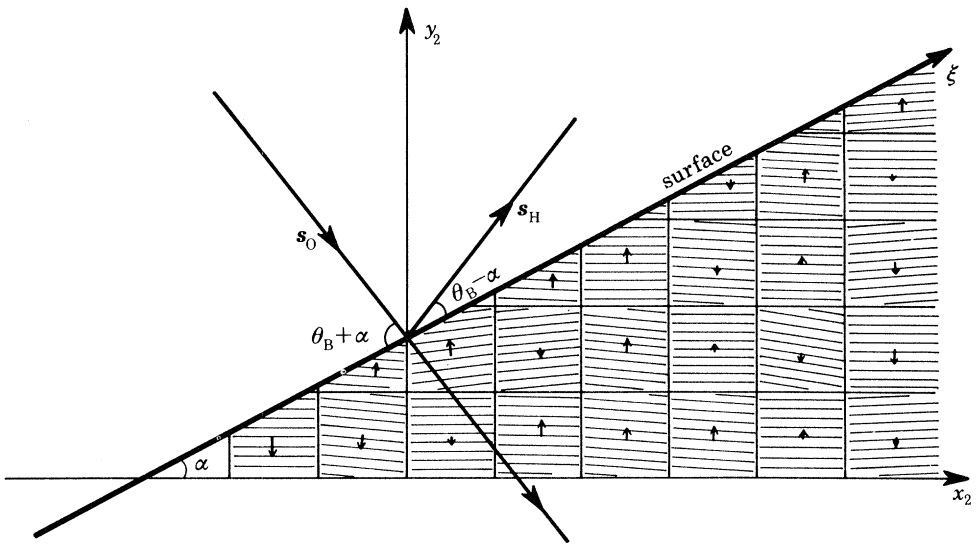

FIGURE 7. Scattering geometry and displacement field for the general mosaic block model in the asymmetric Bragg case with spherical-wave boundary conditions. The tilt of a given block is indicated by the direction of the arrow (which is normal to the Bragg planes of the block). The magnitude of the shift of a block is indicated by the length of the arrow while the sign of the shift is indicated by the sense of the arrow.

(i) *Correlation function for the g.m.b.m.*

The distributions for block tilting and shifting are independent, and the respective contributions to $u_{\|}$ are separate, so we can work out the correlation functions for block tilting and shifting separately. Adopting here the (x_2, y_2) coordinate system (see figure 7), we have the following.

Block-tilt correlation function

$$f_b(\bar{x}_2, \bar{y}_2) \equiv f_b(I\bar{\ell}, J\bar{\ell}) = 2B^{-1}(-1 + \cos B + B\,\mathrm{Si}\,B), \tag{5.5}$$

where

$$B = \sqrt{6}\,\pi\sigma_b H\bar{\ell}, \tag{5.6}$$

Si denotes the sine integral (Abramowitz & Stegun 1965, p. 231) and (I, J) is the difference in block-lattice coordinates between the points in question. Note that f here is independent of (x_2, y_2), since we exclude the case where both sites are in the same block. It immediately follows from (5.5) that $f_b \to 1$ as either σ_b or $\bar{\ell}$ tends to zero, as might be expected.

Block-shift correlation function

$$f_c(\bar{x}_2, \bar{y}_2) \equiv f_c(I\bar{\ell}, J\bar{\ell}) = \exp[-\pi^2 H^2 (I+J)\,\sigma_c^2] \simeq \exp[-C(\bar{x}_2+\bar{y}_2)/\bar{\ell}], \tag{5.7}$$

where

$$C = \pi^2 H^2 \sigma_c^2, \tag{5.8}$$

and we have invoked the Central Limit Theorem of statistics to approximate the sum of several independent, identically distributed random variables by a normally distributed random variable. Note here, also, that $f_c \to 1$ as $\sigma_c \to 0$, as might be expected.

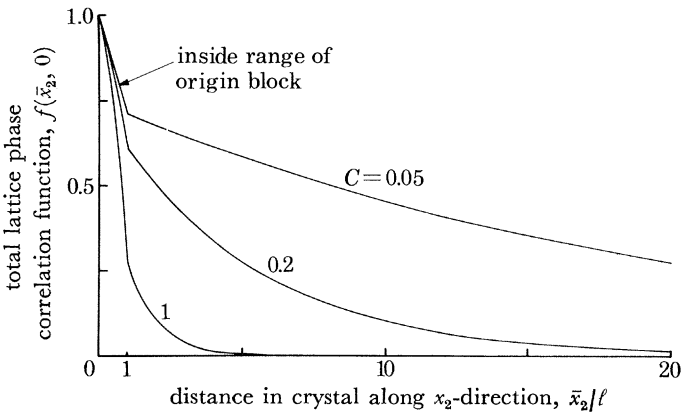

FIGURE 8. Plot of total lattice phase correlation function (given by (5.9)) along the x_2-direction, for $f_b = 0.75$ and for various values of C. The correlation function for $\bar{x}_2 < \bar{\ell}$ involves some correlation from within the origin block, while for $\bar{x}_2 > \bar{\ell}$, only correlation between different blocks is involved.

Total correlation function. Combining (5.5) and (5.6), and taking account of the case where both points in the correlation function lie inside the same block, we obtain for the total function in the g.m.b.m. the result

$$f_t(\bar{x}_2, \bar{y}_2) = \begin{cases} \left(\left(1-\frac{|\bar{x}_2|}{\bar{\ell}}\right)\left(1-\frac{|\bar{y}_2|}{\bar{\ell}}\right) + \left(\frac{|\bar{x}_2|}{\bar{\ell}} + \frac{|\bar{y}_2|}{\bar{\ell}} - \frac{|\bar{x}_2\bar{y}_2|}{\bar{\ell}^2}\right) f_b(\bar{x}_2, \bar{y}_2)\right) f_c(\bar{x}_2, \bar{y}_2) & \\ \qquad \text{for} \quad 0 \leqslant |\bar{x}_2|, |\bar{y}_2| \leqslant \bar{\ell} \quad (5.9a) & \\ f_b(\bar{x}_2, \bar{y}_2) f_c(\bar{x}_2, \bar{y}_2) \quad \text{otherwise,} \quad (5.9b) & \end{cases}$$

where the first term in (5.9*a*) is the probability that points at separation $(\bar{x}_2, \bar{y}_2)$ are in the *same* block, while the prefactor in the second term in (5.9*a*) is the probability that the points at separation $(\bar{x}_2, \bar{y}_2)$ are in *different* blocks.

From the foregoing results we can immediately see that, while the g.m.b.m. crystal is certainly statistically homogeneous, it is *not* statistically isotropic because (5.7) depends on $I+J$ and not on I^2+J^2. An illustration of the form of the correlation function is given in figure 8 and shows that, at small separation distances relative to the block size $\bar{\ell}$, the correlation is near unity and is dominated by the intra-block contribution, while for large distances the correlation falls off exponentially to zero owing to (5.7). That is, there is no infinite-range correlation in the g.m.b.m. provided $C \neq 0$ (cf. Kato 1980).

6. Numerical solution method and format of results

The numerical solution procedure for the T-equations adopted in this work is essentially the same as that described by Authier *et al.* (1968), with the following main differences: (i) boundary conditions are those appropriate to the asymmetric Bragg case with a spherical wave originating on the surface at (0, 0) in the (s_O, s_H) frame; (ii) the numerical iteration procedure makes use only of the preceding values of the field variables d_O, d_H and G_H, and corresponds to method *a* of Authier *et al.* (1968, p. 130). In this case one has the recurrence formulae

$$d_O[(m+1)\,\delta s_O, n\delta s_H] = d_O(m\delta s_O, n\delta s_H) + i(\kappa_{-H}/|\kappa_H|)\,\delta s_O \exp[iG_H(m\delta s_O, n\delta s_H)]\, d_H(m\delta s_O, n\delta s_H), \tag{6.1a}$$

$$d_H[m\delta s_O, (n+1)\,\delta s_H] = d_H(m\delta s_O, n\delta s_H) + i(\kappa_H/|\kappa_H|)\,\delta s_H \exp[-iG_H(m\delta s_0, n\delta s_H)]\, d_O(m\delta s_O, n\delta s_H), \tag{6.1b}$$

with the grid steps being given by

$$\frac{\delta s_O}{\sin(\theta_B-\alpha)} = \frac{\delta s_H}{\sin(\theta_B+\alpha)} = \frac{2\delta\xi}{\sin 2\theta_B}, \tag{6.2}$$

so that grid points lie *exactly* on the surface. The slightly increased level of complication involved in using the recommended method *c* of Authier *et al.* did not seem worthwhile in the present case, because the function G_H in the g.m.b.m. is a *discontinuous* function of position, so the estimate of accuracy for method *c* which they give is probably not reliable. It may be noted that all the methods *a*, *b*, and *c* discussed by Authier *et al.* have the advantage over more subtle methods that they can be used to treat discontinuous G_H-functions.

The essential feature of the numerical solution procedure is that the equations (6.1) are successively solved on 'event lines' (dashed lines in figure 2) yielding diffracted-beam amplitudes on the surface at points $2\delta\xi$ apart, and hence the diffracted-beam intensity profile $I(\xi)$.

Suitable values of $\delta\xi$ for calculating $I(\xi)$ profiles were established by comparing results (see WII) with the corresponding analytical results obtained for a perfect crystal by Uragami (1969), and by comparing results for imperfect crystals obtained with different values of $\delta\xi$. The convergence of spherical-wave integrated reflectivities for a particular value of $\bar{\mu}_0$ (see (4.9)) was established by dividing the integration process up into fixed-length segments (of, say, 160 points), with sequential testing to see if the contribution from the last added segment to the integral was significant. Typically, convergence of integrated reflectivities in this manner to better than 1 % was achieved (see figure 4 in WII), and required from 640 to 960 points on the surface. One may note that the form of (4.9) allows simple calculation of integrated reflectivities for arbitrary larger values of $\bar{\mu}_0$ from the known values of $I(\xi)$ for zero absorption (i.e. one does not have to resolve the T-equations).

For the g.m.b.m., configurations of the distorted crystal were generated from strings of random numbers produced by the Fortran subroutine RANF on the CSIRO Cyber 76 computer. Unless otherwise stated, the string of random numbers used was the same in each case.

Format of results. All results given in §§ 7 and 8 were calculated for a spherical wave originating at (0, 0) on the crystal surface. The quantities plotted are $I(\xi)$ and y^s_{ext} for various values of $\bar{\mu}_0$, β, and the model parameters. In particular, results for $\beta = 0$ and the representative extremely asymmetric case, $(1-\beta^2)^{\frac{1}{2}} = 0.3$, are compared in several graph tableaux (figures 9–13). A crucial result in each tableau is the variation of y^s_{ext} with $(1-\beta^2)^{\frac{1}{2}}$.

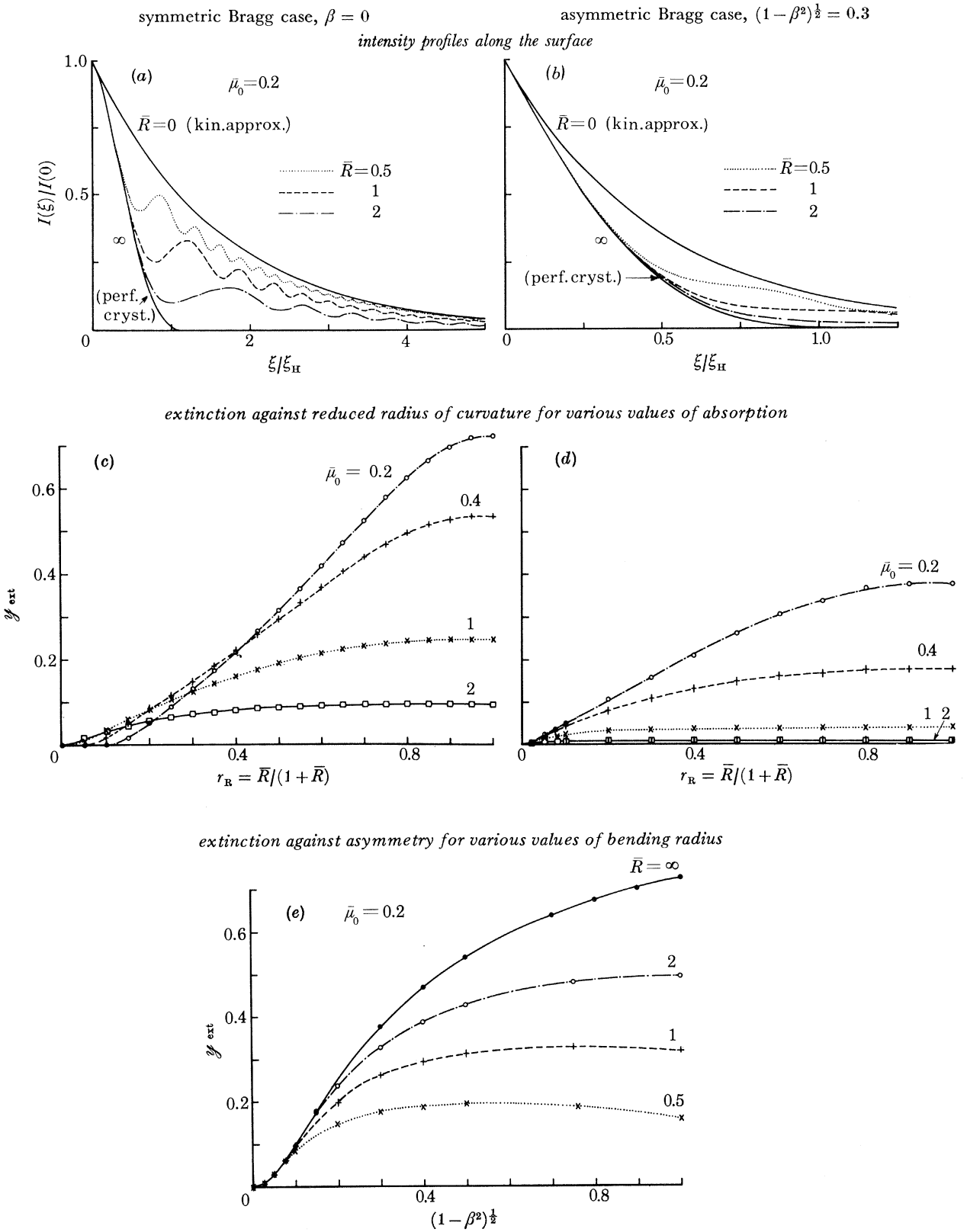

FIGURE 9. Variation of diffraction properties for the uniformly bent crystal in both the symmetric case and a representative extremely asymmetric case. All results are for $\theta_B = \frac{1}{9}\pi$ and $\mathscr{R} = 0$.

The intensity (section-topograph) profiles in each case are plotted in reduced form as $I(\xi)/I(0)$ against ξ/ξ_{H}, where $I(0) = |D\kappa_{\mathrm{H}}/\sin 2\theta_{\mathrm{B}}|^2$, and ξ_{H} is the extinction distance along the surface for a perfect crystal in the Bragg case given by (Uragami 1969)

$$\xi_{\mathrm{H}} = \pi \cos\theta_{\mathrm{B}}/[(1-\beta^2)^{\frac{1}{2}}\,|\kappa_{\mathrm{H}}\kappa_{-\mathrm{H}}|^{\frac{1}{2}}\cos\alpha]. \tag{6.3}$$

7. Results for the uniformly bent crystal†

At the outset, it should be appreciated (see, for example, Chukhovskii *et al.* 1978) that the two ideal limits of scattering are attainable in this model for appropriate limits of the reduced radius of curvature, $\bar{R}$, namely the *dynamical limit* ($\bar{R} \to \infty$) and the *kinematical limit* ($\bar{R} \to 0$). Intensity profiles corresponding to these ideal cases are plotted as solid curves in figure 9.

Figures 9*a and* 9*b*. The intensity profiles given in figure 9*a* for the symmetric case ($\beta = 0$) show that, for all values of $\bar{R}$, the intensity starts off at $\xi = 0$ with the kinematical value, but follows the dynamical profile to an extent depending on the value of $\bar{R}$. The effect of increasing curvature (decreasing $\bar{R}$) is to raise the base level of the Pendellösung fringes and ultimately to increase their spatial frequency (these fringes are manifestations of the waveguide property of diffraction in bent crystals, see, for example, Chukhovskii *et al.* 1978). At large distances from the source point, the intensity again lies close to the kinematical value. Similar results also obtain in the asymmetric case, figure 9*b*, although the decreased spatial frequency of the Pendellösung fringes relative to the symmetric case (see (6.3)) means that attenuation due to normal absorption rapidly damps out the fringes.

Figures 9*c and* 9*d*. Examination of figure 9*c* reveals the perhaps surprising result that, for a given value of $\bar{R}$, the level of extinction can be lower for low absorption cases than for high ones. The explanation for this phenomenon lies in the fact that there are *two regions* where almost kinematical values for $I(\xi)$ are attained, as discussed above, namely for small and large ξ. In the case of low absorption, an increased contribution to scattering is made by the large ξ region, leading to a possible decrease of y_{ext}. This effect is not evident in the asymmetric case (figure 9*d*) because the second kinematical region occurs at much larger values of ξ than for the symmetric case.

Figure 9*e*. Figure 9*e* shows the smooth asymptotic convergence of the various bent-crystal cases to the corresponding perfect-crystal (dynamical-theory) result as the asymmetric limit is approached. It may be noted that variation of y_{ext} with $(1-\beta^2)^{\frac{1}{2}}$ need not be monotonic and, again, this may be ascribed to the relative contributions made by the large- and small-ξ regions.

Simple symmetry arguments, similar to those applied in § 3, may be used to show that (within the framework of the T-equations) the results for $I(\xi)$, and hence y_{ext}, for a uniformly bent crystal are independent of the sign of $\bar{R}$ if $\kappa_{\mathrm{H}} = \kappa_{-\mathrm{H}}$, which is the case in the present study (see (3.15)).

8. Results for the general mosaic block model

(*a*) *Variation of g.m.b.m. parameters*

In most practical cases, the state of a crystal is fixed but not precisely known, and its microstructure can usually only be altered imprecisely and haphazardly (for example, by annealing, α-particle bombardment, thermal shock, polishing and etching,). Such practical techniques do

† See note added in proof, p. 317.

not permit one to study in a controlled fashion diffraction properties as a function of crystal microstructural state, in, say, the approach to the ideally imperfect state (i.e. kinematical approximation) or the perfect state (dynamical theory). It is possible, however, to make a controlled investigation of diffraction properties as a function of crystal microstructural parameters, within the framework of a theoretical calculation, and the present work provides a valuable opportunity for such a study.

One should appreciate that, although $\bar{\ell}$, σ_b and c_c are introduced as independent variables in the g.m.b.m., the variation of any one of them does not necessarily lead to a change in the microstructural state characteristic of that variable alone. This can be seen, for example, by examination of the block-tilt correlation function (5.5) from which it follows that f_b is a function of the block size, $\bar{\ell}$, and, in fact, $f_b \to 1$ as $\bar{\ell} \to 0$ for fixed σ_b. Naively, one might have expected the system to become less correlated as $\bar{\ell} \to 0$ (with $\sigma_c = 0$) rather than more correlated; however, a more careful appraisal in this case shows that $\bar{\ell} \to 0$ implies the blocks become points, and a rotation of a point involves no effective displacement of the medium. When $\sigma_c \neq 0$, one finds that the total correlation function (5.9) is ultimately driven to zero by the block-shift correlation function (5.7), although the tilt correlation function goes to unity. One might equally well have chosen a different set of variables with which to describe the g.m.b.m. The particular choice of parameters is essentially arbitrary, since the continuous variation of any one parameter does not correspond to any particular physical operation that one can perform on a real crystal.

(*b*) *General comments and observations on results*

The figures 10–13 contain compact summaries of the effect on diffraction properties of systematically varying the parameters $\bar{\ell}$ (block-size), σ_b (standard deviation of block-tilt distribution), σ_c (standard deviation of block-shift distribution) and β (the asymmetry parameter). Reference curves also presented in these figures are: (i) for $I(\xi)$ curves, the ideally-imperfect-crystal (kinematical) and perfect-crystal (dynamical) intensity profiles for the same value of the absorption coefficient (solid curves); and (ii) for y_{ext} against asymmetry parameter curves, the perfect-crystal result.

(i) *Hodupicosity*

In all cases the results exhibit features that are idiosyncratic to the particular configuration sampled. Nevertheless, the results also contain features that are representative of the general behaviour of diffraction properties with these parameters (this aspect is investigated in § 8 (*a*i)). The fact that y_{ext} is calculated in the spherical-wave case means that the idiosyncratic behaviour of diffraction with specific crystal microstructure (for the same values of the statistical parameters $\bar{\ell}$, σ_b and σ_c) is extemely severe. At the other extreme of variability with configuration, in the true plane-wave case ($L \to \infty$ in (4.10)), the extinction depends only on the *mean* microstructural state of the crystal, since the plane-wave case averages over an ensemble of spherical-wave cases (i.e. (4.5*b*) with $L \to \infty$). In practice, the incident beam has finite lateral extent, and so idiosyncratic behaviour of extinction with path (see, for example, Mathieson 1977*c*) and sampling volume of crystal (see, for example, Schneider 1977) is inevitable. This phenomenon has been named the *hodupicosian* (from the Greek *hodos* meaning path and *upicos* meaning dependence) character of extinction by Mathieson (1979*b*).

In the figures for y_{ext} presented in this section, the individual data points are presented together with continuous curves through these points. It should, however, be stressed that these curves are

merely introduced as guides to the eye and are *not* meant to imply the existence of any general functional relation between the quantities plotted.

(ii) *The asymmetric limits*

Some important *general* observations based on the present results are that the fine detail in the $I(\xi)$ curves (see figures 9*a*, 10*a*, 11*a*, 12*a* and 13*a*) disappears, as β is varied from the symmetrical case to the asymmetric limits (see figures 9*b*, 10*b*, 11*b*, 12*b* and 13*b*), and that the $I(\xi)$-curves for imperfect crystals tend to approach the corresponding perfect-crystal curve as $\beta \to \pm 1$. For integrated reflectivity data, an extremely strong general observation based on the present results (see figures 9*e*, 10*i*, 11*g*, 12*g* and 13*g*) is the *universal* trend $y_{\text{ext}} \to 0$ as $|\beta| \to 1$, for all imperfect crystal cases studied, which confirms the postulate of Mathieson (1976, 1977*b*). Moreover, in each case, the trend to the kinematical limit is via an asymptotic approach to the dynamical-theory (perfect-crystal) result (as discussed in WII). This is an important finding and opens the way for extrapolation of experimental results via dynamical theory to derive extinction-free values of structure factors (Mathieson 1976, 1977*b*, 1979*a*; WII). The universal nature of these results means we do not have to discuss them in each of the separate cases given below.

(*c*) *Specific observations*

(i) *Variation with configuration*

As discussed in § 8(*b*i), certain features of the calculated results for a given configuration or path are characteristic of that particular configuration or path, and certain features hold generally. To help clarify the separation of the *hodupicosian* and general aspects of the problem, we have investigated the diffraction properties of the g.m.b.m. for the following series of configurations generated by choosing different strings of random numbers.

Configuration 1 is the *standard* or *reference configuration* used in the present work and is based on a given string (say string 1) of random numbers, independent of the particular values of β, $\bar{\ell}$, σ_{b} and σ_{c}.

Configurations 2 *and* 3 involve sampling different configurations of *both* the tilt and shift distributions by using random number strings 2 and 3.

Configurations 4 *and* 5 involve using random number strings such that the tilt component of the configuration is the same as for configurations 2 and 3, respectively, while the shift component is the same as for configuration 1.

Configurations 6 *and* 7 involve using random number strings such that the shift component of the configuration is the same as for configurations 2 and 3, respectively, while the tilt component is the same as for configuration 1.

Observations and comments on variation of results with configuration. Figure 10 consists of a tableau of graphs depicting the variation of diffraction properties with: block-size, $\bar{\ell}$, block-tilt spread, σ_{b}, block-shift spread, σ_{c}, and asymmetry parameter $(1-\beta^2)^{\frac{1}{2}}$, for various configurations. The salient features of these results are as follows.

Figure 10*a*. For $\beta = 0$, the positions of the peaks in the intensity profile $I_{\text{r}}(\xi)$, are essentially the same for all configurations considered, but the relative magnitude of the peaks varies quite drastically from one configuration to another. The results thus imply a well-defined ensemble-average structure for $I(\xi)$ containing peak details characteristic of the g.m.b.m. parameters $\bar{\ell}$, σ_{b} and σ_{c}.

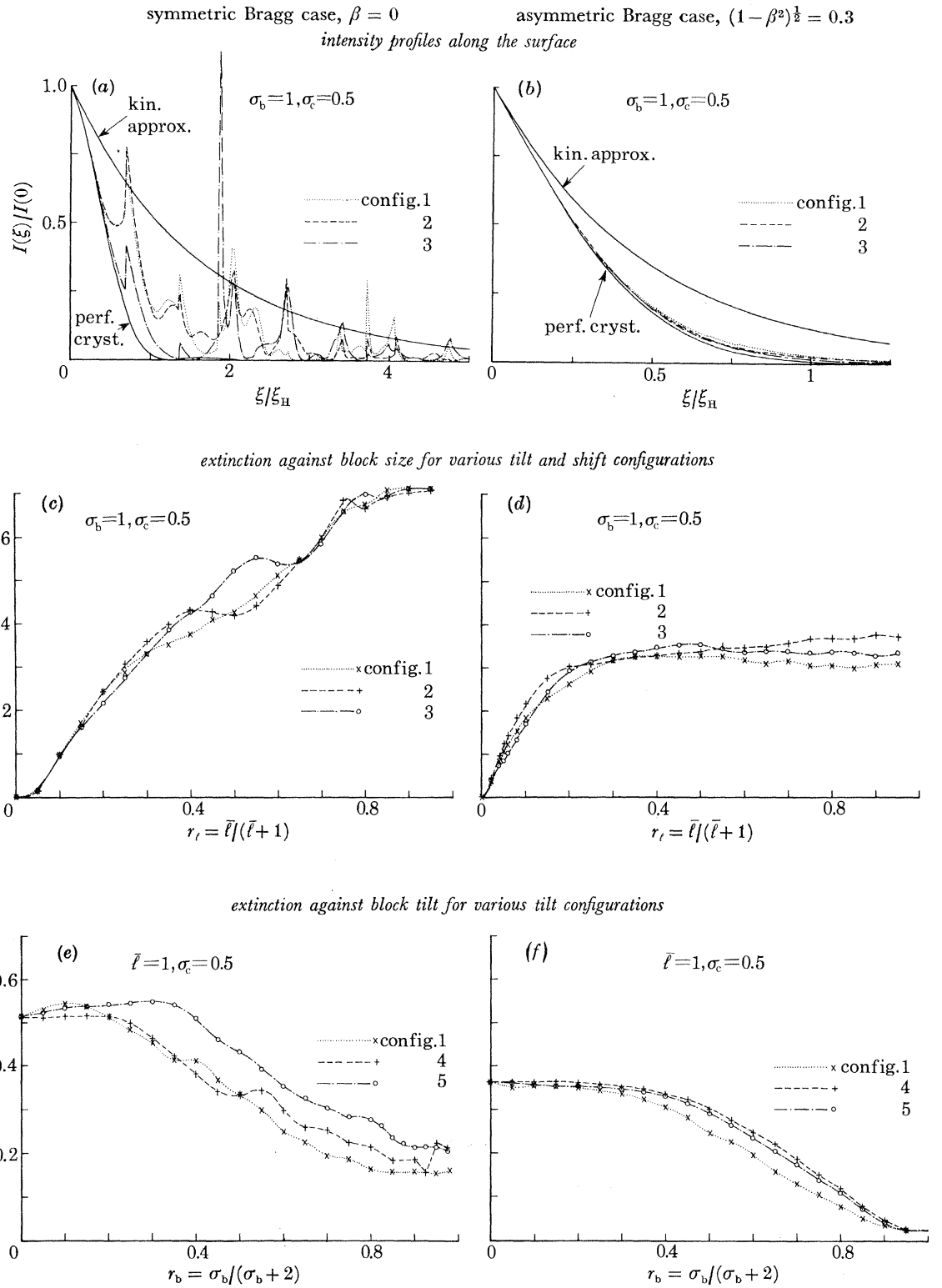

FIGURES 10 (*a–f*). For descriptions see opposite.

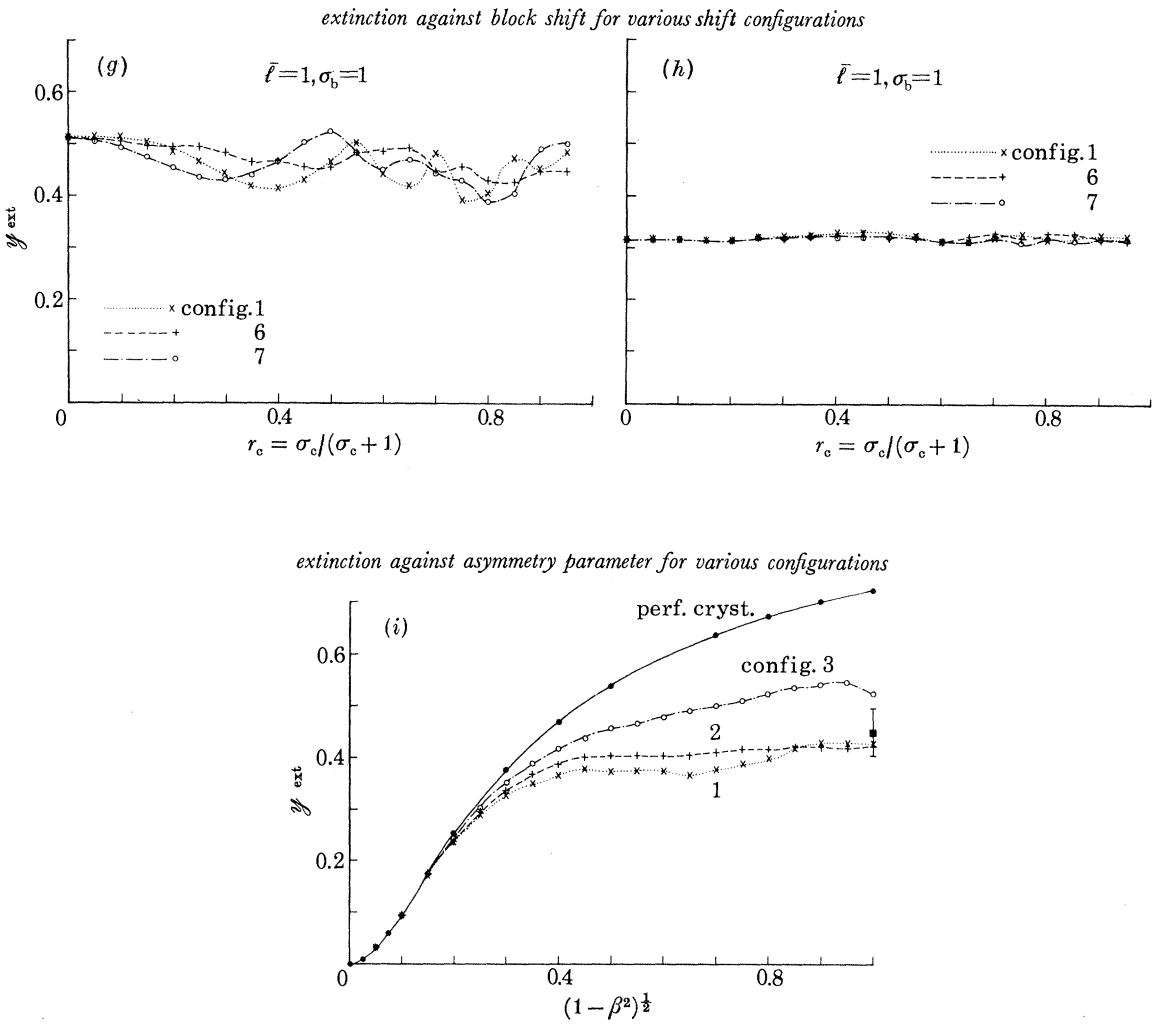

FIGURE 10. Variation of diffraction properties with configuration for the general mosaic block model in both the symmetric case and a representative extremely asymmetric case. All results are for $\bar{\mu}_0 = 0.2$, $\theta_B = \frac{1}{9}\pi$ and $\mathscr{k} = 0$.

Figure 10*b*. For the extremely asymmetric case, the detailed structure in the $I(\xi)$ curves has disappeared and they smoothly follow the perfect-crystal result for all configurations considered.

Figure 10*c*. For the symmetric case, significant dependence on configuration is only shown for intermediate values of $\bar{\ell}$, since for $\bar{\ell}$ small, individual mosaic-block rocking curves of angular width σ_ℓ overlap (i.e. $\sigma_\ell \gtrsim \sigma_b$), and y_{ext} is insensitive to σ_b (type II secondary extinction in the Zachariasen (1967) classification scheme for secondary extinction) while, for $\bar{\ell}$ larger, primary extinction is dominant and this is not affected by the tilt and shift configurations of the blocks.

Figure 10*d*. For the extremely asymmetric case the results for small $\bar{\ell}$ are relatively independent of configuration for the same reasons as given for figure 10*c*. However, for large $\bar{\ell}$ the results in the extremely asymmetric case are complicated by the fact that different configurations involve different effective asymmetry angles, and this effect is significant in the extremely asymmetric régime.

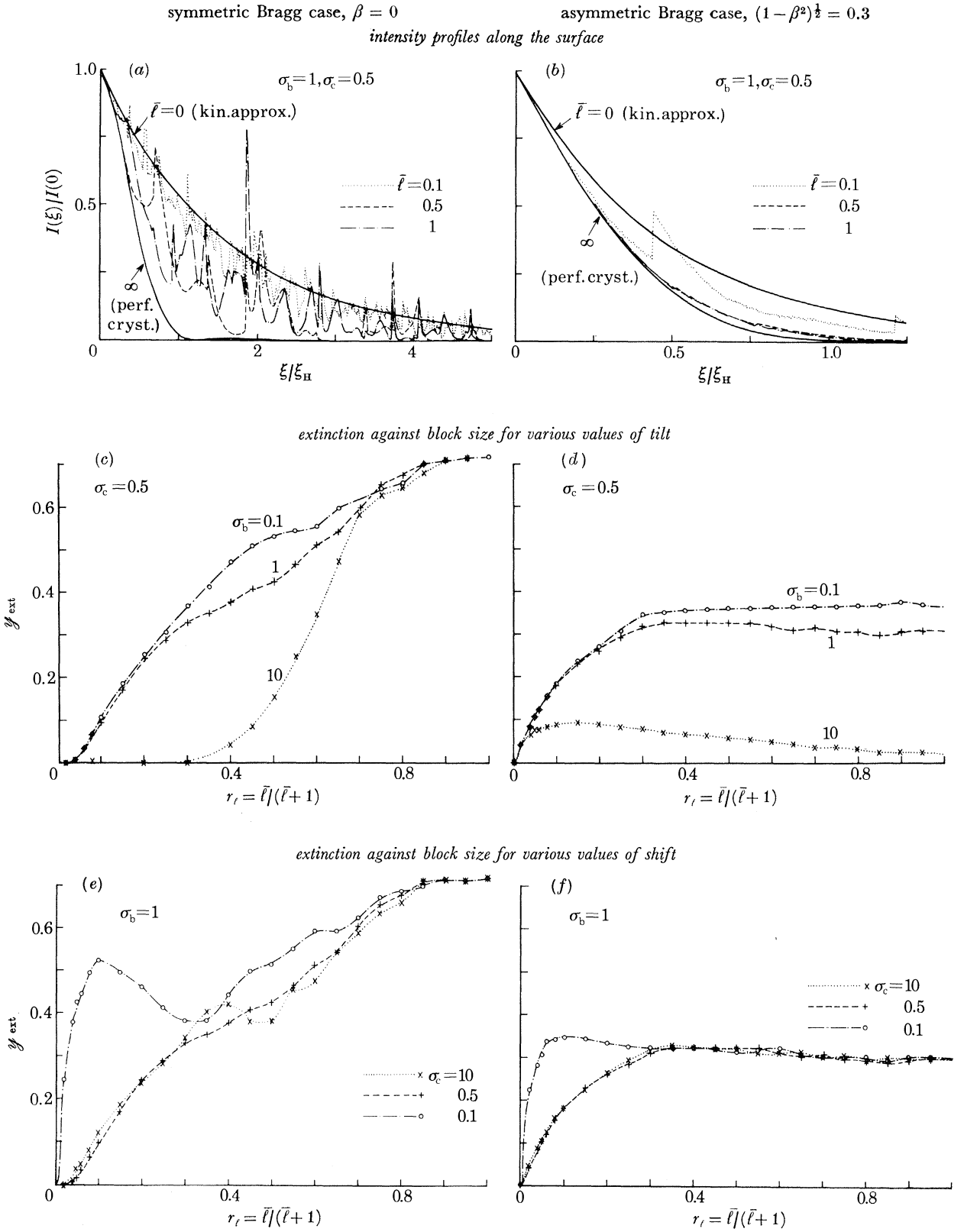

FIGURES 11 (*a–f*). For description see opposite.

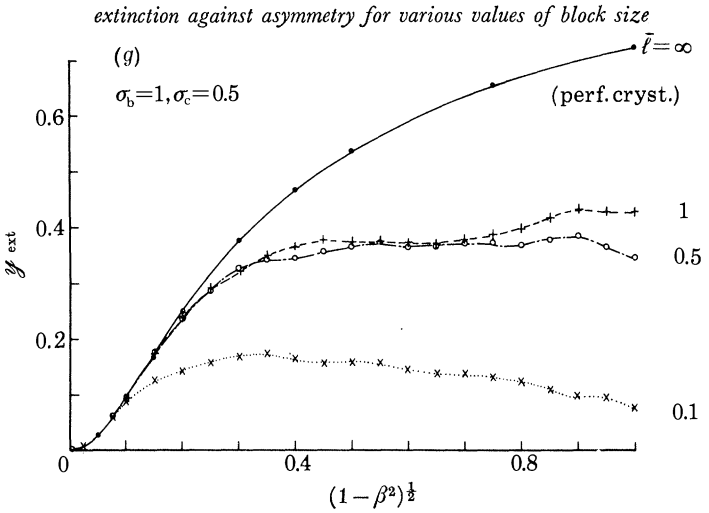

FIGURE 11. Variation of diffraction properties with block-size $\bar{\ell}$ in the general mosaic block model in both the symmetric case and an extremely asymmetric Bragg case. All results are for $\bar{\mu}_0 = 0.2$, $\theta_B = \frac{1}{6}\pi$ and $\kappa = 0$.

Figure 10*e*. For $\beta = 0$, the extinction factor is relatively insensitive to tilt distribution for small values of σ_b because $\sigma_b < \sigma_\ell$, and all blocks are effectively diffraction coupled. However, as σ_b increases, y_{ext} becomes quite sensitive to the particular distribution of tilts, although a well-defined (primary extinction) limit is attained as $\sigma_b \to \infty$ (see also discussion of figures 10*c* and 10*e*).

Figure 10*f*. For the extremely asymmetric case, similar results to those for figure 10*e* obtain, except that the sensitivity to tilt distribution is less severe and the primary extinction limit is effectively zero.

Figure 10*g*. For $\beta = 0$, y_{ext} is insensitive to shift configuration for small σ_c, but shows increasingly large fluctuations in magnitude as σ_c becomes large.

Figure 10*h*. For the extremely asymmetric case, y_{ext} is insensitive to shift distribution for all σ_c.

Figure 10*i*. It can clearly be seen that the sensitivity of y_{ext} to configuration vanishes in the trend towards the asymmetric limits. The vanishing of sensitivity to a particular configuration occurs at almost the same value of β as that at which y_{ext} asymptotically approaches the perfect-crystal result.

The point marked by a square in figure 10*i* denotes the average value of y_{ext}, for $\beta = 0$, obtained by averaging over 10 distinct configurations, and the error bars denote the corresponding sample standard deviation.

(ii) *Variation with block-size* $\bar{\ell}$

Figure 11 consists of a tableau of graphs depicting the variation of diffraction properties with block-size, $\bar{\ell}$. Although some of these results were presented in an earlier work (WII) and a preliminary discussion given there, they are all included here for the sake of completeness. The salient features of these results are as follows.

Figure 11*a*. For $\beta = 0$ and large $\bar{\ell}$ and $I(\xi)$ curves (i.e. for $\bar{\ell} = 0.5$ and $\bar{\ell} = 1$) initially follow the perfect-crystal result ($\ell = \infty$) but, as ξ increases, detailed structure in the curves appears. The smoothly varying dynamical Pendellösung fringes characteristic of highly perfect crystals are not evident in either of these cases. For small $\bar{\ell}$ (say, $\bar{\ell} = 0.1$), the curves are very oscillatory and

lie close to the kinematical-approximation result ($\bar{\ell} = 0$, $\sigma_b = \infty$, and $\sigma_c \neq 0$). Fine structure in the $I(\xi)$ curves appears with a spatial frequency characteristic of the block size. Individual values of $I(\xi)$ exceed the kinematical value in some cases; this is a consequence of treating the scattering problem coherently (similar to occurrence of bright spots in laser speckle patterns, see, for example, Smith 1977).

Figure 11*b*. For the extremely asymmetric case, $(1-\beta^2)^{\frac{1}{2}} = 0.3$, virtually all fine structure in the $I(\xi)$ curves has disappeared and the curves for small block-size ($\bar{\ell} = 0.1$ and 0.5) lie close to the values for a perfect crystal.

Figure 11*c*. Plots of extinction against reduced block size, $r_\ell = \bar{\ell}/(\bar{\ell}+1)$, for $\beta = 0$ show that for small block-size and small spread in block tilts (i.e. small σ_b), the level of extinction is almost independent of σ_b. This is consistent with the notion of wide rocking curves for small mosaic blocks. More specifically, if σ_ℓ is the width of the rocking curve for a block of size $\bar{\ell}$, one expects little variation of y_{ext} with σ_b, for $\sigma_b \lesssim \sigma_\ell$ (corresponds to low primary extinction and type II secondary extinction in the classification scheme of Zachariasen (1967)). For large σ_b one expects almost no secondary extinction and almost pure primary extinction to be present. In figure 11*c*, this case is approximated by the curve $\sigma_b = 10$ (see also figure 14).

For the intermediate region in $\bar{\ell}$, σ_ℓ is sufficiently small such that not all rocking curves for blocks overlap and extinction is a mixture of primary extinction and secondary extinction dominated by the mosaic block distribution, i.e. $\sigma_\ell < \sigma_b$ (type I secondary extinction in Zachariasen's (1967) classification scheme).

For large $\bar{\ell}$, σ_ℓ approaches the perfect-crystal rocking curve width and there is little secondary extinction and almost pure primary extinction.

A further investigation of figure 11*c* is given in § 9.

Figure 11*d*. For the extremely asymmetric case, the results for variation of y^s_{ext} with $\bar{\ell}$ are similar to those in figure 11*c*, except that calculated curves for all values of σ_b coalesce for small $\bar{\ell}$, presumably because of the increased width of the rocking curve in the extremely asymmetric régime (see table I in WI for the perfect-crystal case). Note that y_{ext} tends to different limits for each σ_b value, as $\bar{\ell} \to \infty$, because the infinite blocks will be at different angles to the surface in each case, thus altering the effective asymmetry angle.

Figure 11*e*. For $\beta = 0$, large values of the shift-distribution width, σ_c, and small $\bar{\ell}$, the level of extinction appears largely independent of σ_c. However, if σ_c is small but non-zero, then y_{ext} initially tends towards the perfect-crystal value as $\bar{\ell} \to 0$, before finally tending to zero. This is a consequence of the behaviour of f_t discussed in § 8 (*a*).

The behaviour of y_{ext} in the intermediate region of $\bar{\ell}$ shows that the precise value of σ_c affects the value of y_{ext} to a small but significant degree.

In the trend towards a single perfect-crystal block (i.e. $\bar{\ell} \to \infty$), the value of σ_c becomes irrelevant since intensities are not affected by uniform translation of the whole system (see § 3 (*a*)).

Figure 11*f*. For the extremely asymmetric case, similar results to those obtained in figure 11*e* are found, except that the only region where any sensitivity to σ_c appears to occur is for $\bar{\ell} \to 0$.

(iii) *Variation with block-tilt spread* σ_b

The salient features of figure 12 depicting the variation of diffraction properties with the standard deviation of the block-tilt distribution, σ_b, are as follows.

Figure 12*a*. For $\beta = 0$, the intensity profile $I(\xi)$ shows peaks at positions in ξ characteristic of the block size $\bar{\ell}$, with increasing background value of $I(\xi)$ as σ_b increases. The most spiky $I(\xi)$ curve occurs for the lowest value of σ_b. These results are consistent with the picture of secondary extinction as essentially arising from one block, with nearly 100 % reflectivity in a small angular range, 'shadowing' other blocks further along the path of the incident beam.

Figure 12*b*. For the extremely asymmetric case, the $I(\xi)$ curves for all but the largest value of σ_b smoothly follow the perfect-crystal result. The $I(\xi)$ curve for $\sigma_b = 10$ still lies close to the kinematical result, presumably because the degree of asymmetry is not sufficiently great to cause overlapping of the rocking curves due to asymmetry (see also § 9 (*c*)). All fine detail has been lost from the $I(\xi)$ curves.

Figure 12*c*. For $\beta = 0$ the extinction factor decreases, although not necessarily monotonically, from a large value to a small constant value, as σ_b increases from zero to an indefinitely large value. The asymptotic trend towards a constant value at large σ_b, especially apparent for $\bar{\ell} = 1$, is indicative of the virtual elimination of secondary extinction due to the increased angular spreading-out of the blocks and the attainment of a pure primary-extinction limit (see also the discussion of figure 12*e* and § 9 (*a*i)). It may be noted that y_{ext} does not equal the perfect-crystal value even when $\sigma_b = 0$, because $\sigma_c \neq 0$.

Figure 12*d*. For the extremely asymmetric régime, the primary extinction limit is essentially at $y_{ext} = 0$ for all the values of $\bar{\ell}$ considered.

Figure 12*e*. For $\beta = 0$ the extinction factor starts off at a large value and ultimately decreases to a given constant value as σ_b increases from zero to an indefinitely large value. The uniform attainment of a constant value, independent of σ_c, further provides evidence of the attainment of a pure primary-extinction limit for indefinitely large σ_b.

Figure 12*f*. For the extremely asymmetric case, the primary extinction limit essentially occurs when $y_{ext} = 0$, and so is independent of σ_c.

(iv) *Variation with block-shift spread* σ_c

The salient features of figure 13 depicting the variation of diffraction properties with the standard deviation of the block-shift distribution, σ_c, are as follows.

Figure 13*a*. For $\beta = 0$, the *positions* of the peaks in the intensity profile $I(\xi)$ are essentially independent of σ_c, while the magnitudes of the peaks are affected by the value of σ_c. This is consistent with a picture of σ_c as affecting the relative phasing of different diffracted beams inside the crystal, without altering the essential geometrical conditions for diffraction.

Figure 13*b*. For the extremely asymmetric case, all fine structure in the intensity profile has disappeared, and all curves lie closer to the perfect crystal result ($\sigma_b = 0$ and $\sigma_c = 0$) than the kinematical result.

Figure 13*c*. For the symmetric case, $\beta = 0$, one can see that for large and intermediate values of $\bar{\ell}$ the value of y_{ext} is largely independent of σ_c, which is reasonable, since for such values of $\bar{\ell}$ one expects primary extinction to provide the dominant contribution to y_{ext}. One may also note that for these values of $\bar{\ell}$, the value of y_{ext} oscillates rapidly for large σ_c, since only a few blocks contribute to the diffraction, and the relative phases may change drastically with σ_c.

PHILOSOPHICAL TRANSACTIONS OF THE ROYAL SOCIETY A MATHEMATICAL, PHYSICAL & ENGINEERING SCIENCES

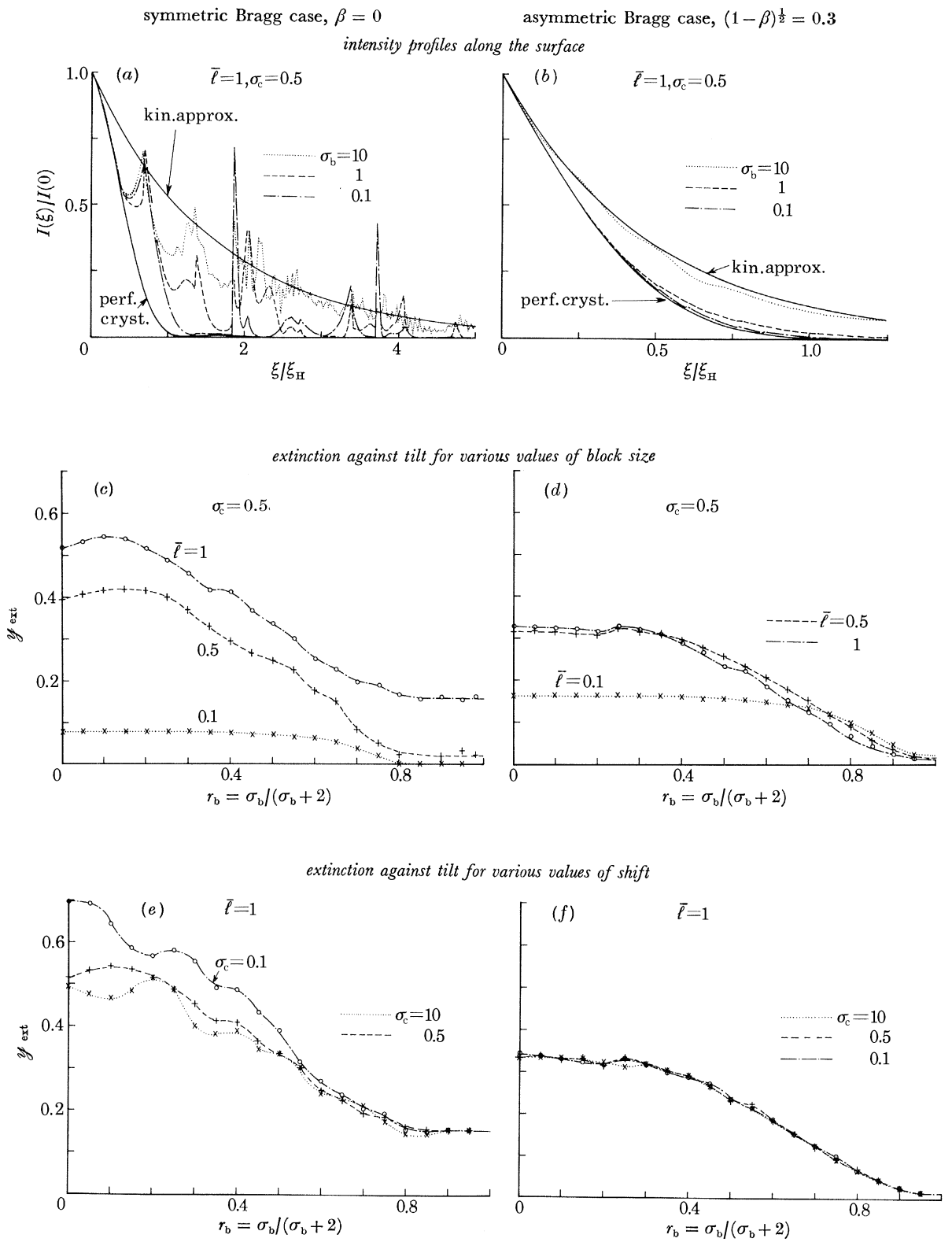

Figure 12 (*a–f*). For description see opposite.

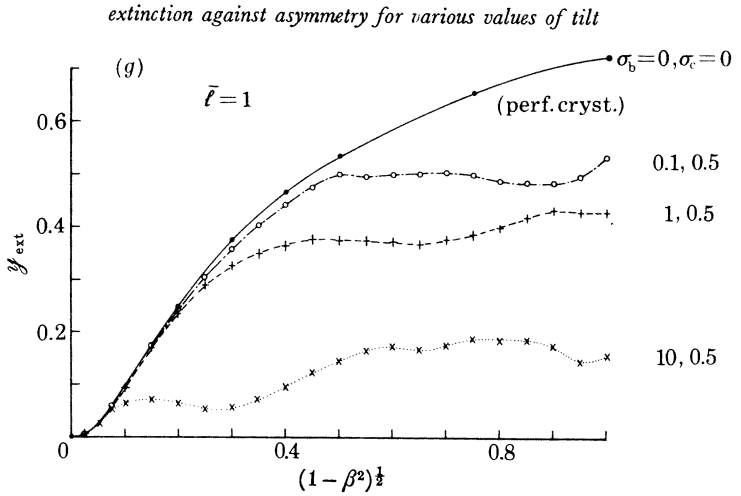

FIGURE 12. Variation of diffraction properties with block tilt spread σ_b in the general mosaic block model in both the symmetric and extremely asymmetric Bragg case. All results are for $\bar{\mu}_0 = 0.2$, $\theta_B = \frac{1}{9}\pi$ and $\ell = 0$.

For small $\bar{\ell}$ one can see that extinction rises rapidly as $\sigma_c \to 0$. This is explained by the fact that the end effect of structurally disordering a crystal by pure tilting becomes small when $\bar{\ell}$ is small, as was discussed in § 8 (*a*). For small $\bar{\ell}$, the fluctuations in y_{ext} for large σ_c are not as great as for large $\bar{\ell}$, probably because there are a large number of blocks with broad rocking curves contributing to the scattering, so that an averaging effect is occurring.

Figure 13 *d*. For the extremely asymmetric case, the results are similar to those found for $\beta = 0$, except that the fluctuations for large $\bar{\ell}$ and σ_c are no longer present. This is consistent with the argument that for the extremely asymmetric case the level of interaction (i.e. g^{-1}, defined in WI) goes to zero, and the angular acceptance or divergence characteristics of the blocks become broad, so that a large number of blocks contribute to the integrated reflectivity (see also § 10 (*c*)).

Figure 13*e*. For the symmetric case and small σ_b, one can see that there is a small reduction in (secondary) extinction as σ_c increases from zero, with the possibility of rapid fluctuations occurring in y_{ext} as σ_c becomes large. On the other hand, for intermediate and large values of σ_b, the level of extinction (mainly primary) is largely independent of σ_c. This is reasonable since σ_c can have no effect on the level of primary extinction.

Figure 13*f*. For the extremely asymmetric case virtually no dependence of y_{ext} on σ_c occurs for any of the values of σ_b considered, and no rapid fluctuations occur for large σ_c. This is presumably due to the fact that large numbers of blocks contribute to the scattering, and relative phasing of blocks is not important.

9. EXTINCTION

(*a*) *Primary and secondary extinction*

The term 'extinction' was introduced into the X-ray diffraction context by Darwin (1922, p. 803) to describe 'the diminution in the reflected beam due to the fact that when one part of a crystal has reflected some of the radiation, there is less for the parts behind it to reflect' (see also Bragg *et al.* 1926). Essentially, the term extinction relates to the failure of the kinematical

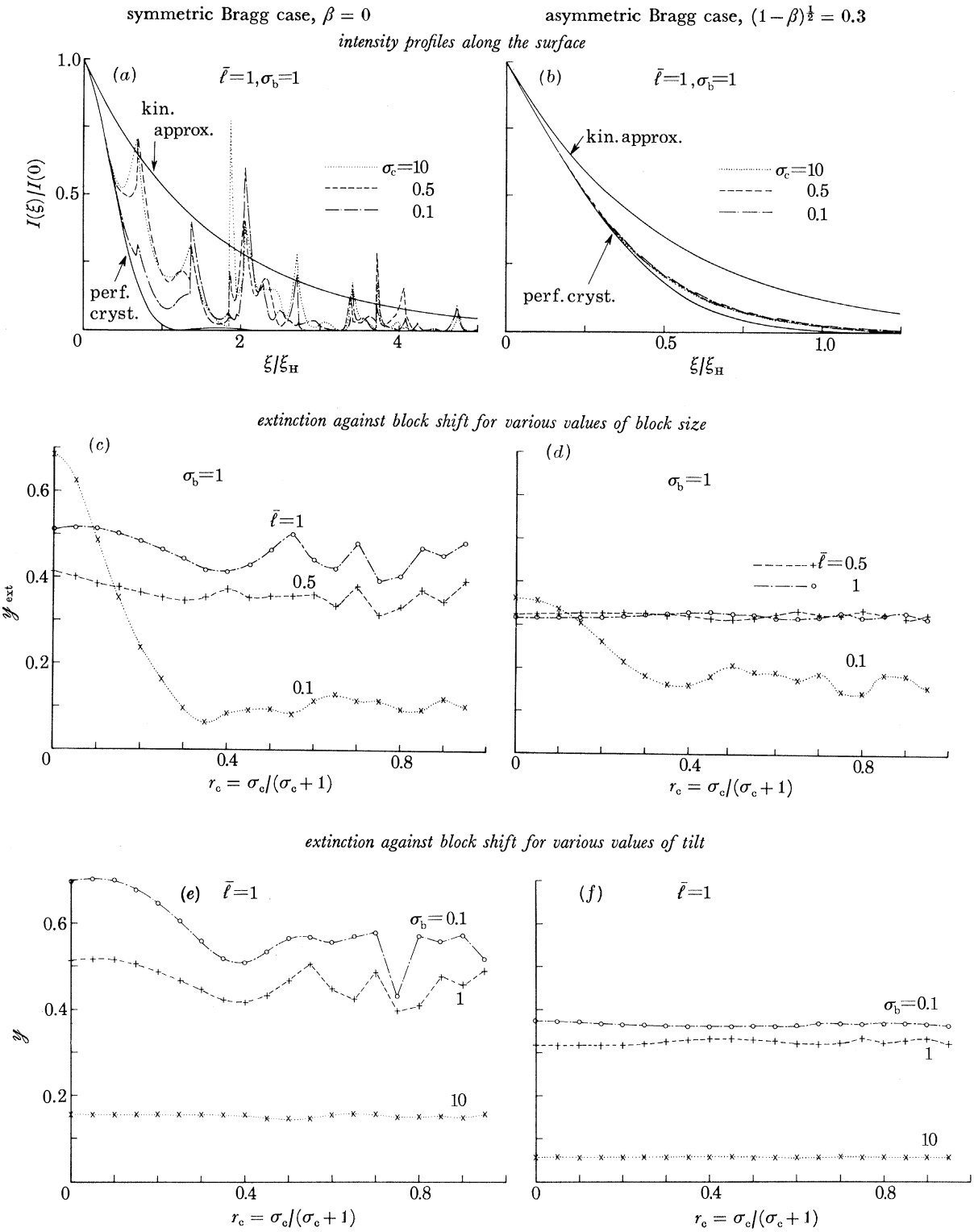

FIGURES 13 (*a–f*). For description see opposite.

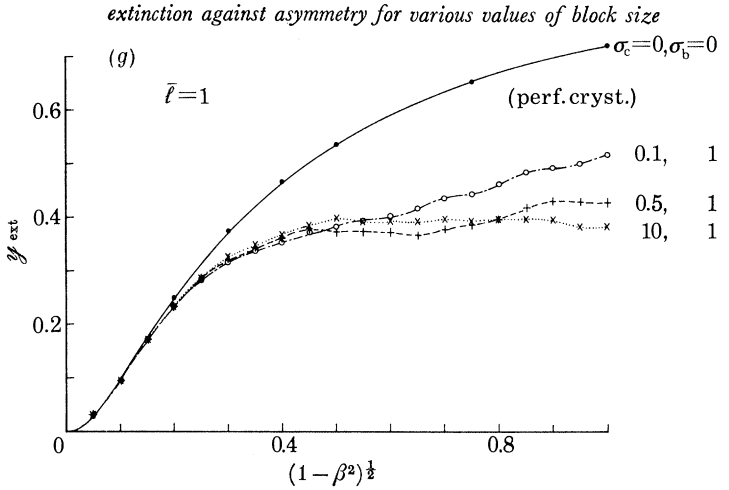

FIGURE 13. Variation of diffraction properties with block shift spread σ_c in the general mosaic block model in both the symmetric and extremely asymmetric Bragg case. All results are for $\bar{\mu}_0 = 0.2$, $\theta_B = \frac{1}{9}\pi$ and $\ell = 0$.

approximation to describe elastic scattering, from real crystals, due to the occurrence of multiple (and even single) Bragg diffraction.

In describing the diffraction process in real crystals, Darwin subdivided the phenomenon of extinction into primary extinction, involving diffraction in an essentially perfect-crystal (coherent) domain ('intrablock scattering'), and secondary extinction, involving the effect of diffraction in one perfect-crystal domain on the scattering from a (incoherent) perfect-crystal domain behind it ('interblock scattering'). The concepts of primary and secondary extinction would seem to be closely tied to a mosaic-block-like picture of an imperfect crystal, where the state of the crystal is perfect over small volumes, but highly distorted on a large scale. It is by no means obvious whether the terms primary and secondary extinction have a useful meaning for describing the structural state of an arbitrary real crystal. In practice, for diffraction from a real crystal, one would expect a clean separation into the two types of extinction to be impossible. Nevertheless, within the framework of the g.m.b.m., it seems possible to use the terms primary and secondary extinction meaningfully, and it is perhaps worthwhile to explore this aspect of the problem.

(i) *Primary extinction*

As was pointed out in the discussion of figures 10*c*, 12*c* and 12*e*, the extinction factor, y_{ext}, tends to a well-defined limit as $\sigma_b \to \infty$, strongly suggesting the attainment of a pure primary-extinction condition in the diffraction experiment. To explore this limiting condition further, we have presented curves of y_{ext} against r_ℓ, for $\sigma_c = 0.5$ and $\sigma_b = 1$ and 100, in figure 14. From the results given earlier, it is reasonable to interpret the y_{ext} curve for $\sigma_b = 100$ as a good estimate for the pure primary extinction curve in the symmetric Bragg case, at least for intermediate and large values of $\bar{\ell}$, since for these values of $\bar{\ell}$ the mosaic-block rocking curves are unlikely to overlap. The effect of a large degree of misorientation of the blocks may be expected to put a severe strain on the accuracy of the numerical solution to the T-equations. For this reason, we have also included values for the $\sigma_b = 100$ case obtained with half the normal spacing in ξ (solid points in figure 14), to give some feeling for the accuracy of the numerical solution.

In addition to the results obtained from the T-equations, we have presented in figure 14 results

for the extinction factor of a crystal, assuming pure primary extinction, obtained by using Darwin's (1922) formula (his equation (6.13); see also Zachariasen (1945), equations (3.167)–(3.169)):

$$Q' = Q \tanh(A)/A, \tag{9.1}$$

for the integrated reflectivity per unit path length, where the path length parameter is given by

$$A = \left(\frac{1+\beta^2\tan^2\theta}{1-\beta^2}\right)^{\frac{1}{2}} \frac{1}{\sin\theta} \frac{e^2\lambda K|F_{\mathrm{H}}|\, t_0}{mc^2 v} = \left(\frac{1+\beta^2\tan^2\theta}{1-\beta^2}\right)^{\frac{1}{2}} \frac{\bar{t}_0}{\sin\theta}. \tag{9.2}$$

We have considered two values of the plate-thickness parameter t_0, namely $t_0 = \ell$ and $t_0 = \ell \sin\theta$.

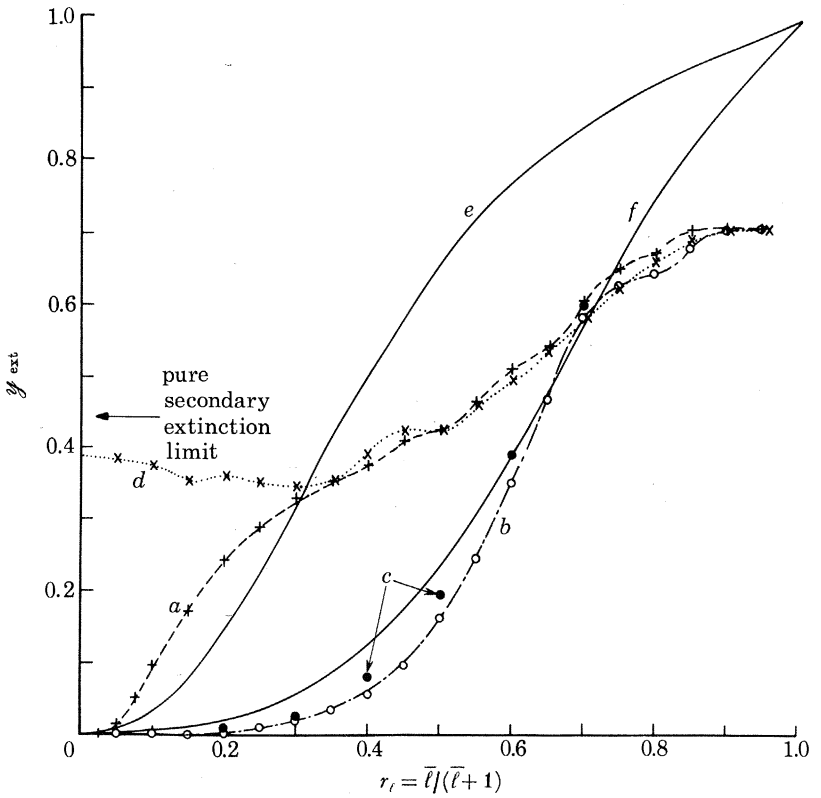

FIGURE 14. Plot of extinction factor $y^{\mathrm{s}}_{\mathrm{ext}}$ against block size: *a*, A moderately disordered mosaic crystal, namely the g.m.b.m. with $\sigma_{\mathrm{b}} = 1$, $\sigma_{\mathrm{c}} = 0.5$ (- - - +). *b*, A highly misoriented mosaic crystal, namely the g.m.b.m. with $\sigma_{\mathrm{b}} = 100$, $\sigma_{\mathrm{c}} = 0.5$ (—·—·○). This curve essentially represents the form of pure primary extinction in the g.m.b.m. for $\bar{\mu}_0 = 0.2$, $\theta_{\mathrm{B}} = \frac{1}{9}\pi$ and $\mathscr{k} = 0$. *c*, Same case as for *b*, but with half the grid-spacing in the numerical solution procedure (●). *d*, A mosaic crystal with shift spread $\sigma_{\mathrm{c}} = \bar{\ell}^{\frac{1}{2}}\sigma^0_{\mathrm{c}}$ and $\sigma^0_{\mathrm{c}} = 0.5$ (· · · ×). This curve tends to a pure secondary-extinction limit as $\bar{\ell} \to 0$. *e*, Predictions of the Darwin result (equation (9.1)) for pure primary extinction (and $\bar{\mu}_0 = 0$) with $t_0 = \ell$ and *f*, the corresponding curve with $t_0 = \ell \sin\theta_{\mathrm{B}}$ (——). Unless otherwise stated, all results are for $\bar{\mu}_0 = 0.2$, $\theta_{\mathrm{B}} = \frac{1}{9}\pi$ and $\mathscr{k} = 0$.

The pure primary extinction factor for the crystal is calculated by replacing Q by Q' in (4.14), where Q' is given by (9.1), and the extinction factor by (4.15), so that

$$y^{\mathrm{prim}}_{\mathrm{ext}}(\mathrm{Darwin}) = 1 - \tanh(A)/A, \tag{9.3}$$

which is independent of μ_0. It can be seen from figure 14 that the result for a crystal with pure primary extinction calculated in the Darwin approximation, with the obvious identification $t_0 = \ell$, does not agree at all well with the numerical result obtained via the T-equation. The value

of y_{ext} obtained from the Darwin formula is much larger than the numerical result. This may be traced to the fact that the Darwin result treats the diffraction from blocks via the theory for an infinite parallel plate of thickness t_0 in the case of negligible absorption.

On the other hand, if one interprets the quantity $t_0(1+\beta^2\tan^2\theta)^{\frac{1}{2}}/(1-\beta^2)^{\frac{1}{2}}\sin\theta$ as the effective linear dimension of a crystal block (see Zachariasen 1945, p. 135), one has for the symmetrical case the relation $t_0 = \bar{\ell}\sin\theta$ (or equivalently $A = \bar{\ell}$). The resulting plot of $y_{\mathrm{ext}}^{\mathrm{prim}}$(Darwin) is shown in figure 14, where it can be seen that this choice for t_0 leads to reasonably close agreement with the corresponding numerical result for $y_{\mathrm{ext}}^{\mathrm{prim}}$, at least for small and intermediate values of $\bar{\ell}$. At large $\bar{\ell}$, the effect of absorption inside each block becomes significant and the validity of the assumptions underlying the simple Darwin treatment is expected to break down (see, for example, Becker 1977).

As an adjunct to the present discussion of primary extinction, one may note that while $y_{\mathrm{ext}}^{\mathrm{prim}}$ is clearly *dependent* on the parameters $\bar{\mu}_0$, β, θ_{B}, K and λ, it is *independent* of σ_{b} and σ_{c}.

(ii) *Secondary extinction*

It follows by definition that any additional contribution to the total extinction in excess of that contributed by primary extinction is due to secondary extinction. While primary extinction is relatively easy to discuss conceptually, secondary extinction is much more difficult. In particular, the level of secondary extinction in the g.m.b.m. clearly depends in general on all three parameters: $\bar{\ell}$, σ_{b} and σ_{c}. Moreover, it is clear that the level of secondary extinction is, in general, affected by the level of primary extinction. The method by which one could attain a well-defined pure secondary-extinction state is perhaps not obvious within the present formulation of the g.m.b.m., although such a state would be attained for $\bar{\ell}\to 0$ with

$$\sigma_{\mathrm{c}}(\bar{\ell}) = \bar{\ell}^{\frac{1}{2}}\sigma_{\mathrm{c}}^0, \tag{9.4}$$

where σ_{c}^0 is independent of $\bar{\ell}$. The choice (9.4) for σ_{c} was arrived at by requiring a constant standard deviation in the field-point displacement (i.e. $u_{\parallel}$ given by (5.4)) per unit length in the crystal due to block-shift alone. The results for (9.4) with $\sigma_{\mathrm{c}}^0 = 0.5$ and $\sigma_{\mathrm{b}} = 1$ are presented as crosses joined by a dotted curve in figure 14. From these results it can be seen that for large $\bar{\ell}$ there is little dependence on the form of σ_{c}, which is reasonable since primary extinction is predominant, while for small $\bar{\ell}$ one can see that y_{ext} tends to a non-zero limit as $\bar{\ell}\to 0$. In this latter case, primary extinction is zero and one has *pure secondary extinction*.

In addition to the behaviour in the limit $\bar{\ell}\to 0$, one knows that the levels of secondary extinction must go smoothly to zero as $\bar{\ell}\to\infty$, since the type of extinction is gradually becoming more nearly primary as one approaches the perfect-crystal limit (see figure 14).

It is not obvious how one may provide a rigorous mathematical approach to the calculation of the level of secondary extinction in the diffraction from an imperfect crystal in which primary extinction is also occurring. Perhaps an easier approach is to *define* the level of secondary extinction via the commonly adopted relation (see, for example, Becker & Coppens 1974, p. 133)

$$\frac{\rho_{\mathrm{tot}}}{\rho_{\mathrm{kin}}} = \frac{\rho_{\mathrm{sec}}}{\rho_{\mathrm{kin}}}\frac{\rho_{\mathrm{prim}}^{\mathrm{b}}}{\rho_{\mathrm{kin}}^{\mathrm{b}}} \Leftrightarrow 1 - y_{\mathrm{ext}}^{\mathrm{tot}} = (1-y_{\mathrm{ext}}^{\mathrm{sec}})\,(1-y_{\mathrm{ext}}^{\mathrm{prim}}), \tag{9.5}$$

where integrated reflectivities without superscripts refer to the entire crystal, while those having the superscript b refer to values calculated for a single mosaic block.

(*b*) *Extrapolation to the asymmetric limits and the determination of extinction-free structure-factor values*

The theoretical results for imperfect crystals presented in §§ 7 and 8 lend very strong support to the approach suggested by Mathieson (1976, 1977*b*) for eliminating the effect of extinction from measured intensities or structure factors, by systematic *extrapolation* of such data to the asymmetric (extinction-free) limits. Moreover, from the present work, one has the very useful result that the most appropriate mathematical form for the extrapolation of integrated reflectivity data to the asymmetric limits is the perfect-crystal or dynamical-theory result (see also WII), even though the limit itself is the kinematical value.

Practically, an extinction-free determination of a structure factor, from integrated reflectivity data at a series of values of β, could proceed by first using that data to calculate, via standard dynamical theory for a perfect crystal (see, for example, Hirsch & Ramachandran 1950; Wilkins 1978*a*, *b*), a measured value for the structure factor, say $F_{\mathrm{meas}}(\beta)$ (or, more correctly, a measured value for the parameter $\overline{\mu}_0$, or equivalently g_0, both defined in equations (3.17), as a parameter of this form actually occurs in the dynamical theory, rather than F alone). Secondly, the values of $F_{\mathrm{meas}}(\beta)$ could then be extrapolated, as, say, a function of $(1-\beta^2)^{\frac{1}{2}}$, to zero, and the limiting value of F_{meas}, say F^0_{meas}, would in principle be free from extinction.

A current limitation on the absolute accuracy of the above method for determining structure-factor values is the fact that one really determines only, say, $\overline{\mu}_0$, and this is essentially the ratio of the linear absorption coefficients, μ_0, to the modulus of the structure factor $|F_{\mathrm{H}}|$, and μ_0 is not accurately known for most substances. Nonetheless, one would certainly have extinction-free *relative* values for structure factors.

An interesting alternative way of using extrapolation to the asymmetric limit would be to use a known value of $|F_{\mathrm{H}}|$ for a system to determine μ_0 from the extinction-free measurement of g_0 for that system. Such a method would avoid one of the main difficulties in conventional determinations of μ_0, namely the accurate measurement of crystal thickness.

From the present results, it can be seen that the task of extrapolating measured data to obtain an extinction-free estimate for g_0 is facilitated by working with crystals that are as nearly perfect as possible. Thus, one requires accurately flat, nearly perfect crystal surfaces for study. One approach to the preparation of such surfaces would be to progress through an ever diminishing cycle of fine polishing, followed by mild etching of the surface, or preferably to use a chemical polish.

(*c*) *Nature of the diffraction process in the approach to the asymmetric limits*

From the results presented in figures 9–13, two very striking and apparently universal effects occur as the degree of asymmetry tends to the limits:

(i) the intensity profile, $I(\xi)$, becomes smoothly varying with ξ, and the values of $I(\xi)$ become independent of the precise mosaic structure;

(ii) the integrated reflectivity tends asymptotically to the value calculated in the conventional dynamical theory for a perfect crystal, and this result in turn tends to the kinematical value at the asymmetric limits.

Because of the form of the T-equations chosen for solution, it is not practical to obtain a detailed picture of the diffraction process inside the crystal as a function of angle. However, from a knowledge of the diffraction behaviour of perfect-crystal scattering volumes in the approach to the asymmetric limit (Wilkins 1978*a*, see in particular the summary of the effects of asymmetry

given in table I) and from general principles, such as the Liouville theorem applied to the spatial and angular spreads of the beams (Albertini *et al.* 1977), it is possible to make some reasonable guesses as to the underlying physical factors leading to the effects (i) and (ii) described above.

First, it should be noted that the degree of asymmetry has a pronounced effect on the relative cross sections of the incident and diffracted beams (see figure 1). This effect was first noticed in X-ray powder diffraction effects by Stephen & Barnes (1935, 1936), who found that powder diffraction lines 'making a small angle with the surface of the specimen are particularly sharp, but become broader as the angle between the diffracted beams and the surface of the specimen increases' (i.e. decreasing positive asymmetry), although primacy for observing this effect is often mistakenly given to Fankuchen (1937). In the negative asymmetry case, a corresponding spatial expansion of the diffracted beam occurs relative to the incident. In each case, the effect is essentially geometrical in origin (see figure 1). Concomitant with a spatial expansion (or contraction) of the beam in direct space is a corresponding decrease (or increase) in the angular divergence of the diffracted beam, as the asymmetry parameter, β, tends to the negative (or positive) asymmetric limit. For a perfect crystal, a simple geometrical description of this effect can be given in terms of the dispersion surface (see, for example, Schwarz & Cohen 1977, p. 502), and is analogous to the foreshortening effect in direct space. The relation between the two effects may be viewed as a manifestation of the Liouville theorem (Albertini *et al.* 1977). It should be noted that the condensation effects in direct and reciprocal space are essentially geometric in origin and so should be independent of the state of the crystal.

Secondly, it is known from the perfect-crystal case studied earlier (Wilkins 1978*a*) that the *level of interaction* $g^{-1} \approx 4t_{\mathrm{abs}}/t_{\mathrm{ext}}^{\mathrm{prim}}$, where t_{abs} is the absorption length in the absence of diffraction, while $t_{\mathrm{ext}}^{\mathrm{prim}}$ is the extinction length in the absence of absorption, goes to zero in the asymmetric limits. That is, the distance between successive scattering events is, on average, large compared to the absorption length. Moreover, for imperfect crystals, one expects the level of interaction for a given crystal at a given value of β to be even lower than for the corresponding perfect crystal.

Thirdly, one also knows from the perfect-crystal case that in the limit $\beta \to -1$ the *rocking curve width becomes indefinitely large* and the maximum reflectivity goes to zero, while for the limit $\beta \to +1$ the *angular divergence* of the diffracted beam becomes indefinitely large, and the maximum reflectivity also goes to zero.

If one assumes that similar diffraction effects also occur for an imperfect crystal, then for the case $\beta \to -1$ one may interpret the asymptotic convergence of the integrated reflectivity for an imperfect crystal to that for perfect a crystal as arising because the level of interaction, g^{-1}, is going to zero, so that the probability of multiple scattering within a block is going to zero (i.e. primary extinction in the conventional sense is going to zero), together with the fact that the rocking curve width is such that each block is diffraction-coupled to every other block in the scattering path (i.e. $\sigma_\ell > \sigma_{\mathrm{b}}$). In the secondary extinction classification scheme of Zachariasen (1967), this situation corresponds to type II secondary extinction, although here we see that, in the trend to the asymmetric limit, this ultimately corresponds to primary extinction for the whole crystal treated as one block.

For the case $\beta \to +1$, the level of interaction also goes to zero, but it is the *angular divergence range* of the scattering function for a block which becomes indefinitely large, leading to diffraction coupling between all blocks in a given scattering path (see figure 15). Conventionally (see Darwin 1922; Zachariasen 1967; Becker & Coppens 1974), the scattering function for a block is calculated for a given angle of incidence, but integrated over all angles of scattering (corresponding to

a rocking curve), so that, in the treatment of diffraction from an imperfect crystal, one ignores the spreading-out of the two beams as they pass through the crystal (see, for example, Darwin 1922, p. 818). Thus, the form of secondary extinction exhibited in the trend $\beta \to +1$ does not fit into the conventional classification scheme, although it may logically be called type III secondary extinction. In the limit $\beta \to +1$, secondary extinction of type II also becomes equivalent to primary extinction for the whole crystal treated as one block.

The fact that the angular divergence or acceptance characteristic of each block is becoming indefinitely large would also explain why the intensity profile becomes smooth as $|\beta| \to 1$.

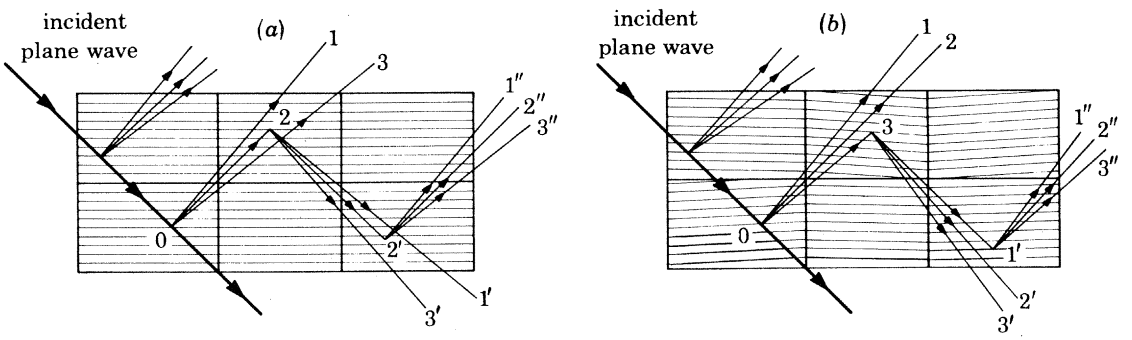

FIGURE 15. Diffraction process in the extremely asymmetric Bragg case $\beta \to \pm 1$ for (*a*) a perfect crystal and (*b*) an imperfect crystal, in each case showing angular spreading-out of the diffracted beam. The scattering series 0–2–2′ for the perfect crystal is different from the corresponding series 0–3–1′ for the imperfect crystal, but, for an approximately uniform angular response function for the diffracted power in the crystal, the net diffracted intensity will be approximately equal in each case. The form of interblock coupling, arising via angular spreading-out of the diffracted beam, is here termed secondary extinction type III.

(*d*) *Relation of the present work to theories for correcting for the effect of extinction*

The thrust of the present work in regard to the extinction problem is in line with the philosophy recently expounded by Mathieson (1979*a*) involving *elimination* of extinction by making a series of measurements under *controlled* variation of adjustable physical parameters, followed by appropriate extrapolation of the data to a well-defined extinction-free limit. This approach, however, involves more extensive data collection than is usually made. For experiments where only a small number of measurements of each reflexion are made, or where the experiment has not been designed to allow a suitable extrapolation procedure, there is still a need for theories, albeit approximate, for *correcting* for the effect of extinction (see, for example, Darwin 1922; Werner & Arrott 1965, Werner *et al.* 1966; Zachariasen 1967; Becker & Coppens 1974; Kato 1976*b*; Becker 1977), since the task of numerically solving the T-equations for an imperfect crystal is too time-consuming to be incorporated practically within a cycle of a conventional least-squares refinement routine. Moreover, there is the additional difficulty that direct comparisons between theory and experiment by using the T-equations would seem to require ensemble averages of both the numerical calculations and the experimental data, to overcome the problem of hodupicosity (see § 8 (*b*i)).

Work of the present type may, however, provide a very valuable means for *testing the accuracy of different extinction theories* for a wide variety of imperfect crystals and experimental conditions. That conventional extinction theories can only follow to a limited extent the predictions of the T-equations for the g.m.b.m., follows from the fact that the g.m.b.m. is described by three independent parameters (ℓ, σ_b and σ_c), while conventional extinction theories have at most two

parameters. In particular, it may be noted that Darwin-like theories involve parameters of the type $\bar{\ell}$ and σ_b, but do not have a parameter resembling the block-shift spread, σ_c. This parameter describes the degree of correlation (coherence) between the origins of different blocks, whereas the Darwin-like theories, involving intensity-coupling equations, effectively assume no correlation (incoherence) between the origins of different blocks.

(i) *Types of extinction*

The results presented here demonstrate that the type of extinction present is, in general, not just a function of the structural state of the crystal, but is also dependent on the parameters defining the diffraction experiment, such as β, λ, K, μ_0 and θ_B. Thus, one should refer, for example, to a type II experiment, rather than to a type II crystal (cf., for example, Cooper 1979; Cooper *et al.* 1979).

It may also be pointed out here that the Zachariasen (1967) classification scheme for extinction into either types I or II was found inadequate in the discussion of § 9 (*d*). The reason for this inadequacy was the failure of that scheme to consider the degree of spreading-out of the diffracted beam in the crystal, and this suggests that the similar assumption made by Darwin (1922, p. 818) and his followers in deriving their extinction theories may not always be valid.

10. Conclusions and prospects

The present work provides strong evidence for the universal nature of the asymmetric limits as limits where the diffraction behaviour is *independent* of the particular microstructural state of the crystal specimen. Moreover, it has been found that, for a large class of imperfect crystal cases, the diffraction quantities $I(\xi)$, ρ and y_{ext} all tend asymptotically to the dynamical values appropriate to a single perfect crystal as the asymmetric limits are approached, and that these quantities in turn tend to the kinematical values at the limit (see also Wilkins 1980). Although the present results were derived for the case of zero anomalous dispersion (i.e. $\ell = 0$), our previous work on perfect crystals (WI) suggests that the universal nature of the limit also obtains for $\ell \neq 0$.

The methods used in the present work offer possibilities for

(i) investigating the nature of other extinction-free limits for imperfect crystals (see Mathieson 1976, 1977*a*, *b*, 1979*a*);

(ii) testing the accuracy of approximate extinction theories (see, for example, Kato 1976*a*, *b*, 1979, 1980);

(iii) analysis of section topographs from highly imperfect crystals by comparing ensemble-averaged data and numerical results;

(iv) aiding in the design of X-ray and neutron optical devices (see, for example, Hart 1971), including the use of imperfect crystals (see, for example, Hart & Rodrigues, 1979);

(v) treating the problem of dynamical scattering from surfaces and layer structures (see, for example, Betekhtin *et al.* 1978);

(vi) studying the wavefield inside imperfect crystals, for example, to calculate fluorescence yields (see, for example, Kruglov & Shchemelev 1978);

(vii) treating arbitrarily shaped imperfect crystals.

I am extremely grateful to Dr A. McL. Mathieson for arousing my interest in this study and for continued advice and encouragement in its exploration. I am also grateful to Mr A. F. Moodie for helpful discussion, and to Dr S. L. Mair for her comments on the manuscript.

PHILOSOPHICAL TRANSACTIONS OF THE ROYAL SOCIETY A MATHEMATICAL, PHYSICAL & ENGINEERING SCIENCES

References

Abramowitz, M. & Stegun, I. A. 1965 *Handbook of mathematical functions*, pp. 231. New York: Dover.
Albertini, G., Boeuf, A., Lagomarsino, S., Mazkedian, S., Melone, S. & Rustichelli, F. 1977 *Acta crystallogr.* A **33**, 360.
Authier, A. 1977 In *X-ray optics* (ed. H. J. Queisser). Berlin: Springer-Verlag.
Authier, A., Malgrange, C. & Tournarie, M. 1968 *Acta crystallogr.* A **24**, 126.
Barrett, C. S. & Massalski, T. B. 1966 *Structure of metals*. New York: McGraw-Hill.
Bragg, W. L., Darwin, C. G. & James, R. W. 1926 *Phil. Mag.* **1**, 897.
Bragg, W. L., James, R. W. & Bosanquet, C. H. 1921*a* *Phil. Mag.* **41**, 309.
Bragg, W. L., James, R. W. & Bosanquet, C. H. 1921*b* *Phil. Mag.* **42**, 1.
Becker, P. J. 1977 *Acta crystallogr.* A **33**, 243.
Becker, P. J. & Coppens, P. 1974 *Acta crystallogr.* A **30**, 129.
Betekhtin, V. I., Ivanov, S. A. & Mal'chuzhenko, K. V. 1978 *Soviet Phys. solid State*, **20**, 2067.
Boeuf, A., Melone, S., Puliti, P. & Rustichelli, F. 1978 *J. appl. Crystallogr.* **11**, 265.
Chukhovskii, F. N., Gabrielyan, K. T. & Petrashen, P. V. 1978 *Acta crystallogr.* A **34**, 610.
Chukhovskii, F. N. & Petrashen, P. V. 1977 *Acta crystallogr.* A **33**, 311.
Cooper, M. J. 1979 *Acta crystallogr.* A **35**, 176.
Cooper, M. J., Sakata, M. & Rouse, K. D. 1979 *Acta crystallogr.* A **35**, 250.
Darwin, C. G. 1914*a* *Phil. Mag.* **27**, 315.
Darwin, C. G. 1914*b* *Phil. Mag.* **27**, 675.
Darwin, C. G. 1922 *Phil. Mag.* **43**, 800.
Fankuchen, I. 1937 *Nature, Lond.* **139**, 193.
Goodman, P. 1975 *Acta crystallogr.* A **31**, 804.
Hart, M. 1971 *Rep. Prog. Phys.* **34**, 435.
Hart, M. 1974 International Crystallography Conference: *Diffraction studies of real atoms and real crystals*, p. 318. Canberra: Australian Academy of Science.
Hart, M. & Rodrigues, A. R. D. 1979 *Phil. Mag.* **40**, 149.
Hashizume, H. & Kohra, K. 1971 *J. phys. Soc. Japan* **31**, 204, 1124.
Hirsch, P. B. 1956 *Prog. Metal Phys.* **6**, 236.
Hirsch, P. B. & Ramachandran, G. N. 1950 *Acta crystallogr.* **3**, 187.
James, R. W. 1948 *The optical principles of the diffraction of X-rays*. London: Bell and Sons.
Katagawa, T. & Kato, N. 1974 *Acta crystallogr.* A **30**, 830.
Kato, N. 1961 *Acta crystallogr.* A **14**, 627.
Kato, N. 1968 *Acta crystallogr.* A **24**, 157.
Kato, N. 1973 *Z. Naturf.* **28**, 604.
Kato, N. 1974 In *X-ray diffraction* (ed. L. V. Azaroff). New York: McGraw-Hill.
Kato, N. 1975 *Proceedings of International Summer School on X-Ray Dynamical Theory and Topography*, Limoges, France.
Kato, N. 1976*a* *Acta crystallogr.* A **32**, 453.
Kato, N. 1976*b* *Acta crystallogr.* A **32**, 458.
Kato, N. 1979 *Acta crystallogr.* A **35**, 9.
Kato, N. 1980 *Acta crystallogr.* A **36**, 763.
Kohra, K., Ando, M. & Matsushita, T. 1978 *Nucl. Instrum. Meth.* **152**, 161.
Kruglov, M. V. & Shchemelev, V. N. 1978 *Soviet Phys. solid St.* **20**, 1385.
Kuriyama, M. 1970 *Acta crystallogr.* A **26**, 56.
Kuriyama, M. 1972 *Acta crystallogr.* A **28**, 588.
Kuriyama, M. & Miyakawa, T. 1970 *Acta crystallogr.* A **26**, 667.
Laue, M. von 1935 *Ann. Phys.* **23**, 705.
Lawrence, J. L. & Mathieson, A. McL. 1977 *Acta crystallogr.* A **33**, 288.
Lorentz, H. A. 1905 *Proc. Sect. Sci. K. ned. Akad. Wet.* **8**, 401.
Mathieson, A. McL. 1975 *Acta crystallogr.* A **31**, 769.
Mathieson, A. McL. 1976 *Nature, Lond.* **261**, 306 (erratum: *Nature, Lond.* **262**, 236).
Mathieson, A. McL. 1977*a* *Acta crystallogr.* A **33**, 133.
Mathieson, A. McL. 1977*b* *Acta crystallogr.* A **33**, 610.
Mathieson, A. McL. 1977*c* *Acta crystallogr.* A **35**, 288.
Mathieson, A. McL. 1978 *J. appl. crystallogr.* **11**, 163.
Mathieson, A. McL. 1979*a* *Acta crystallogr.* A **35**, 50.
Mathieson, A. McL. 1979*b* Private communication.
Messiah, A. 1965 *Quantum mechanics*, vol. II. Amsterdam: North-Holland.
Moodie, A. F. 1972 *Z. Naturf.* **27**, 437.
Moodie, A. F. & Warble, C. E. 1980 (To be published.)
Petrashen, P. V. & Chukhovskii, F. N. 1976 *Soviet Phys. JETP* **42**, 243.

PHILOSOPHICAL TRANSACTIONS OF THE ROYAL SOCIETY A MATHEMATICAL, PHYSICAL & ENGINEERING SCIENCES

Petrashen, P. V. & Chukhovskii, F. N. 1978 *Soviet Phys. solid St.* **20**, 637.
Pinsker, Z. G. 1978 *Dynamical scattering of X-rays*. Berlin: Springer-Verlag.
Pogany, A. P. & Turner, P. S. 1968 *Acta crystallogr.* A **24**, 103.
Saka, T., Katagawa, T. & Kato, N. 1972 *Acta crystallogr.* A **28**, 102.
Schneider, J. R. 1977 *Acta crystallogr.* A **33**, 235.
Schwarz, C. H. & Cohen, J. B. 1977 *Diffraction from materials*. New York: Academic Press.
Smith, H. M. 1977 *Holographic recording materials*. Berlin: Springer-Verlag.
Stephen, R. A. & Barnes, R. J. 1935 *Nature, Lond.* **136**, 793.
Stephen, R. A. & Barnes, R. J. 1936 *Nature, Lond.* **137**, 532.
Takagi, S. 1962 *Acta crystallogr.* **15**, 1311.
Takagi, S. 1969 *J. phys. Soc. Japan* **26**, 1239.
Tanner, B. K. 1976 *X-ray diffraction topography*. Oxford: Pergamon Press.
Taupin, D. 1964 *Bull. Soc. fr. Minér. Inst.* **87**, 469.
Uragami, T. S. 1969 *J. phys. Soc. Japan* **27**, 147.
Warren, B. E. 1969 *X-ray diffraction*. Reading, Massachusetts: Addison-Wesley.
Werner, S. A. & Arrott, A. 1965 *Phys. Rev.* **140**, 675.
Werner, S. A., Arrott, A., King, J. S. & Kendrick, H. 1966 *J. appl. Phys.* **37**, 2343.
Wilkins, S. W. 1978*a* *Proc. R. Soc. Lond.* A **364**, 569. (WI.)
Wilkins, S. W. 1978*b* *Acta crystallogr.* A **34**, 343.
Wilkins, S. W. 1980 *Acta crystallogr.* A **36**, 143. (WII.)
Zachariasen, W. H. 1945 *Theory of X-ray diffraction in crystals*. New York: John Wiley.
Zachariasen, W. H. 1967 *Acta crystallogr.* A **23**, 558.

Note added in proof, 10 *October* 1980. Recent measurements of Bragg-case section topographs for perfect crystals (Lang, A. R. & Mai, Z. H. 1979, *Proc. R. Soc. Lond.* A **368**, 313) and uniformly bent crystals (Papoyan, A. A. Aladzhadzhyan, N. M. & Bezirganyar, p. 8, 1980, *Sov. phys. crystallogr.* **25**, 225) appear consistent with the calculations reported in §7.

PHILOSOPHICAL TRANSACTIONS OF THE ROYAL SOCIETY A MATHEMATICAL, PHYSICAL & ENGINEERING SCIENCES